Space Science and Engineering Center
University of Wisconsin–Madison

**A REPORT
OF THE
SEVERE WEATHER PROGRAM
FOR THE PERIOD
1 SEPTEMBER 1991 TO 31 AUGUST 1992**

A REPORT from the

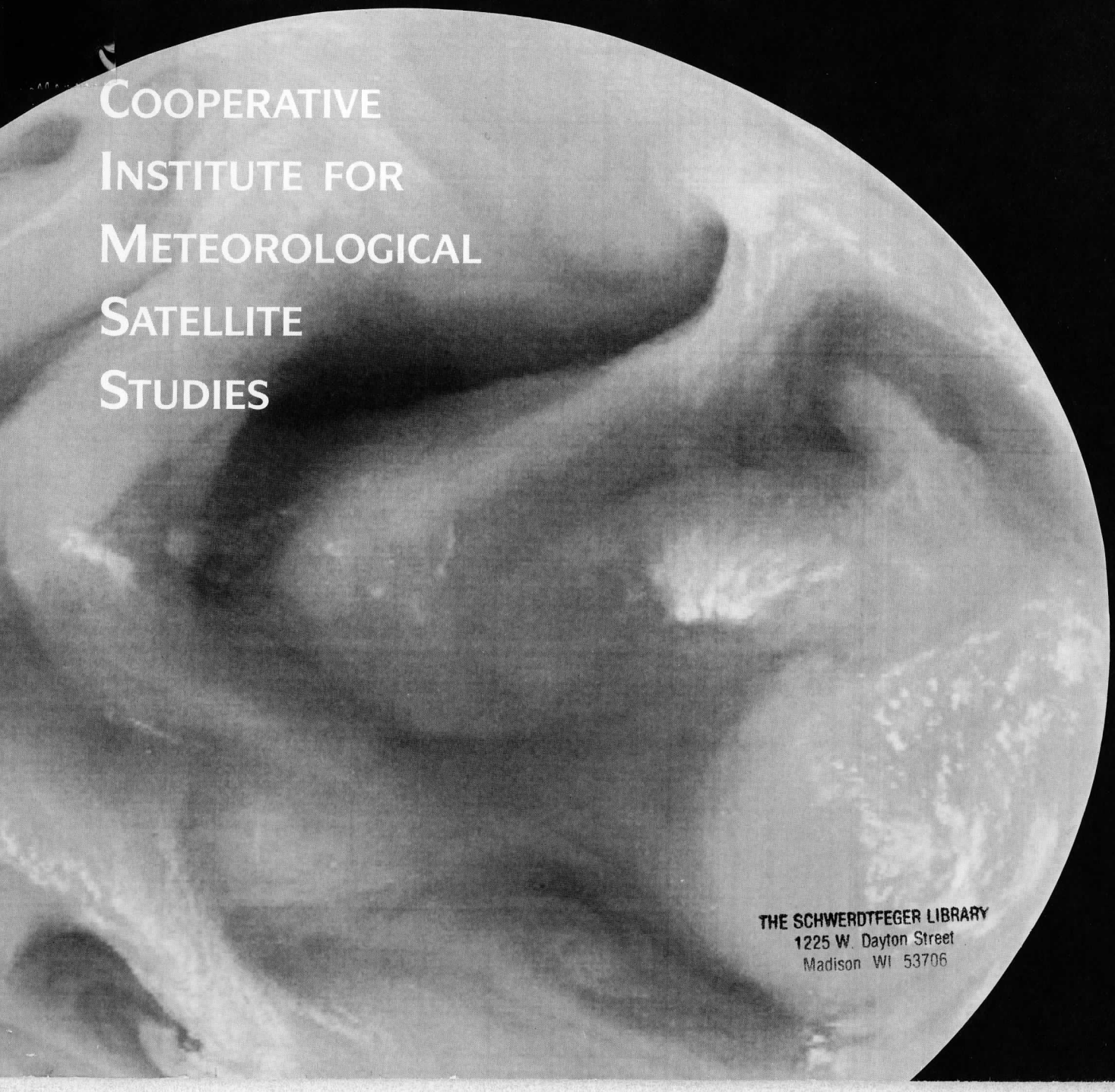

COOPERATIVE INSTITUTE FOR METEOROLOGICAL SATELLITE STUDIES

A REPORT
OF THE
SEVERE WEATHER PROGRAM
FOR THE PERIOD
1 SEPTEMBER 1991 TO 31 AUGUST 1992

Submitted by

Cooperative Institute for Meteorological Satellite Studies
Space Science and Engineering Center (SSEC)
at the University of Wisconsin-Madison
1225 West Dayton Street
Madison, Wisconsin 53706
(608) 263-7435

William L. Smith
Director, CIMSS
Principal Investigator

Anthony J. Schreiner
Associate Researcher
Program Manager

Christopher M. Hayden
Chief, SDAB
Principal Scientist

TABLE OF CONTENTS

I. INTRODUCTION

This annual report discusses the work completed during the final year of a three year funding period. The period covered is from 1 September 1991 through 31 August 1992. The scope of this report is twofold. Section II provides a brief summary of the results and accomplishments successfully completed during the contract period. Section III describes the number of personnel and the newly acquired equipment needed to accomplish the goals detailed in the results section (Section II). Sections IV and V summarize and list all the references, respectively. The Reference section includes all the references in the Results section plus articles resulting from the research work.

The main areas covered in this report are:

- The Gulf of Mexico Experiment (GUFMEX) - Two studies examining the distribution and evolution of atmospheric moisture in the Gulf of Mexico. The first uses GOES VISSR Atmospheric Sounder (VAS) data, while the second examines total precipitable water and surface wind speed from the Special Sensor Microwave/Imager aboard the polar orbiting Defense Meteorological Satellite Platform (DMSP) series.
- Data assimilation - Two areas are covered under this topic. The first looks at the assimilation of diabatic heating and cloud liquid water. A second study examines the Bayesian statistical principles and their application towards data assimilation.
- STORM-FEST - A detailed listing of archived data for the STORM-FEST (1 February 1992 - 14 March 1992) is included. This includes both remotely sensed information plus surface data and numerical model fields. From these, data modeling impact studies are planned. A discussion of the CIMSS Regional Assimilation System (CRAS) and preliminary results are included.
- Polar orbiting products - Because the time intervals in the overlapping regions of the AVHRR data are on the order of 100 minutes, an investigation, using image information from NOAA-11 and NOAA-12, was performed to reduce the relatively large time interval between images. The resulting smaller time difference improved the quantity and maintained the quality of the satellite measured cloud motion vectors.
- Interpolation of surface skin temperature utilizing satellite data, surface observations, and a simple diurnal forcing function - The calculation of accurate skin temperature is critical in the application of satellite-derived radiance information. Differences between the calculated skin temperature and the observed surface temperature can vary greatly due to the effects of diurnal forcing and the different observation times of the two data sources. A simple diurnal forcing model, which attempts to compensate for the different observation times, was tested.
- The Southwest Area Monsoon Project (SWAMP) - A study of the evolving moisture fields over the southwestern United States was performed for data gathered during August of 1990. Data from both VAS dwell sound and MSI radiance data, and dropsonde data from the NOAA P-3 were used.

II. RESULTS

A. OBTAINING CLOUD MOTION VECTORS OVER THE ARCTIC FROM AVHRR.

Contribution by Leroy D. Herman

Large gaps in the meteorological network in the Arctic and Antarctic can be filled by obtaining wind patterns using polar orbiting satellite AVHRR data. The method uses techniques similar to the GOES method of measuring cloud motion vectors. However, there are several differences between the two methods. First, the pictures must be rectified to a standard map projection. Second, the time interval between consecutive passes of the NOAA satellites is approximately 100 minutes. Third, visible pictures are only available during the Arctic summer, necessitating working with infrared data during the rest of the year. Fourth, the temperature of the surface is much colder than at tropical latitudes, with land surfaces usually covered by snow, while the ocean is covered by ice. Each of these differences involves problems which are unique to high latitudes (Turner and Warren, 1989 and Herman, L. D., 1991).

An investigation was made into the feasibility of using two different satellites to obtain cloud motion vectors over a shorter interval instead of using all data from a single satellite. Since NOAA-11 and NOAA-12 are designed to provide afternoon and morning coverage respectively, at high latitudes the two orbits cross. Those orbits which are closest in time are the ones in which we are most interested. Careful examination of these times of orbit crossing shows the interval is not constant, but instead varies in a cyclic manner over a ten day period. During this period the orbits vary from being in synchronization at the start, through a time difference of 50 minutes after five days, to being in synchronization again at the end of ten days.

A case was selected on March 19, 1992 where the interval between passes over Ellesmere Island was close to 50 minutes, and over 100 cloud motions were measured. The measurements at both 100 minute and 50 minute intervals showed good agreement in the flow patterns, indicating a 100 minute interval is acceptable. Figure 1 shows the cloud patterns over a four hour period of rectified and enhanced NOAA-11 and NOAA-12 images.

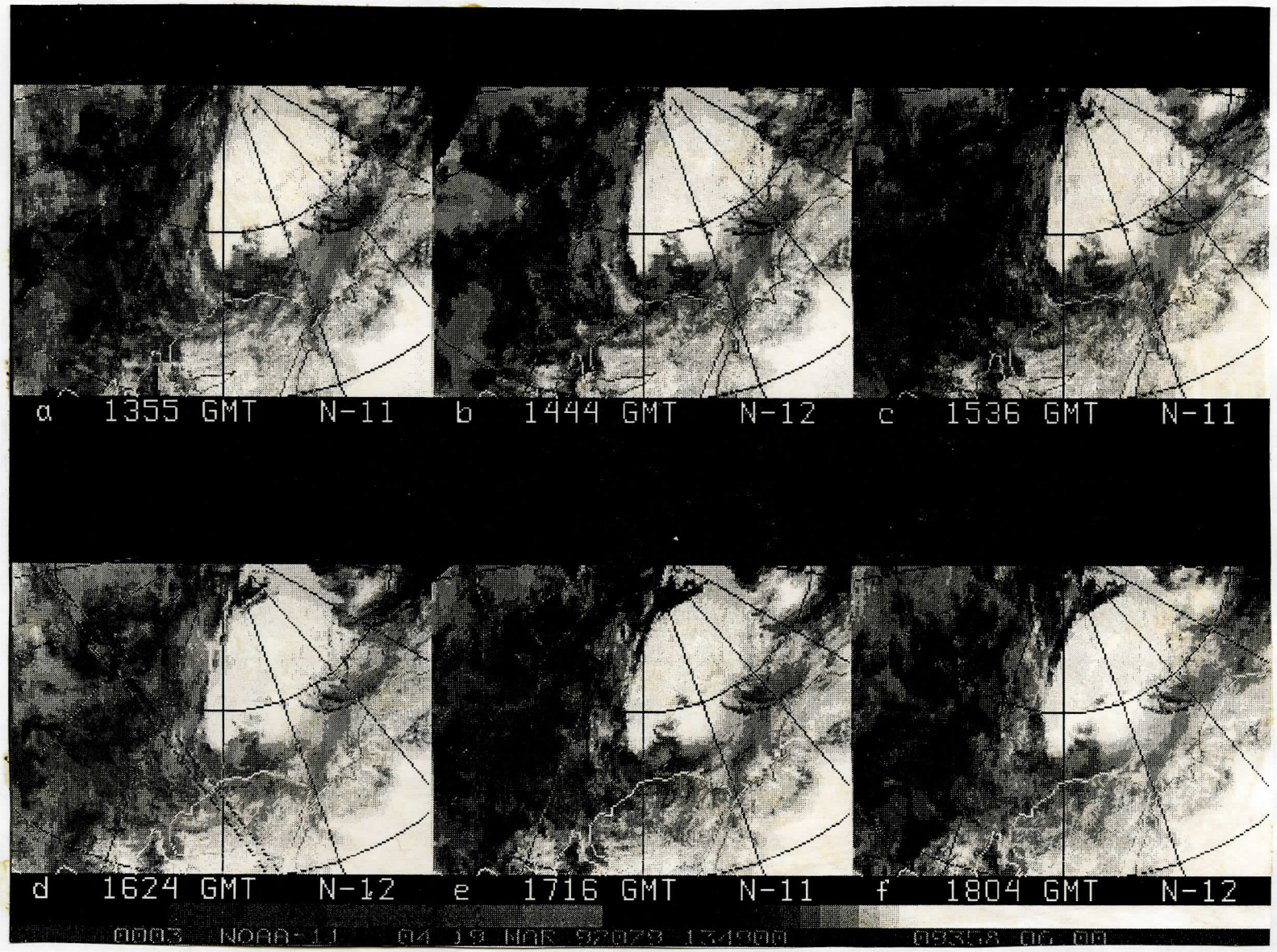

Figure 1. Cloud patterns for a four hour period over Ellesmere Island on 19 March 1992 for NOAA-11 and NOAA-12.

B. ATMOSPHERIC MOISTURE IN THE GULF OF MEXICO. Contribution by Robert M. Rabin.

Two studies concentrated on the distribution and evolution of atmospheric moisture in the Gulf of Mexico. The first study investigated spatial and temporal changes in the vertical distribution of atmospheric water vapor during a period following the intrusion of cold continental air over the Gulf of Mexico, during the Gulf of Mexico Experiment (GUFMEX) in February-March 1988 (Rabin, et al., 1992). Infrared satellite measurements from the GOES VISSR Atmospheric Sounder (VAS) were used to augment the sparse coverage of rawinsonde sites in the vicinity of the Gulf of Mexico. Precipitable water from two vertical layers, surface-850 hPa and 850-250 hPa, were estimated from the VAS and compared to those from rawinsonde observations. The accuracy of precipitable water estimates in each vertical layer was found to be less than that for the total precipitable water. However, improvements in the estimate of precipitable water for each layer were observed with respect to the profiles used in initializing the retrieval process. A consistent horizontal and temporal pattern of the vertical partition of water vapor between the lower and middle to upper troposphere was obtained from the analysis in both layers. A band of moist air which developed with return to southerly flow was common to both layers, however the width of the band was more extensive in the lower layer. Drying to the rear of the band predominated in the upper layer while the lower layer remained quite moist.

In the second study (Rabin, et al., 1993), the atmospheric water budget was examined for a 12-day period following an intense cold air outbreak over the Gulf of Mexico. Budget terms were compared using analyses from the U.S. National Meteorological Center's operational Nested Grid Model (NGM) and using precipitable water and surface wind speed estimated from the Special Sensor Microwave/Imager (SSM/I) instrument aboard the Defense Meteorological Satellite Platform (DMSP).

The atmospheric storage term, determined from the areal averaged total precipitable water, did not differ significantly between that obtained from the NGM and that obtained from SSM/I data. The storage increased by a factor of more than 3 during the initial 5 days following the passage of the surface high over the Gulf. Horizontal flux divergence of water vapor computed from the full vertical structure in the NGM output was found to be well approximated by the substitution of the surface-700 hPa mean wind and the total precipitable water for the vertical profiles along the boundaries of the atmospheric volume. Evaporation from the sea surface was determined using GOES satellite surface temperatures and NGM surface air conditions. The impact of satellite derived surface winds on the areal average evaporation was determined by replacing NGM wind speeds with those estimated from the SSM/I data. The relative importance of precipitation on the water budget was assessed from model estimates. During the onset of air mass modification, evaporation appeared to be the dominant mechanism in producing the observed atmospheric moistening. As evaporation diminished after 1 to 2 days, evaporation and flux convergence became of similar magnitude. Together, these terms underestimate the amount of moistening observed during the first 5 days.

C. THE VAS STORM-FEST ARCHIVE. Contribution by Timothy J. Schmitt.

During STORM-FEST, the available VAS data, ancillary data, intermediate and final products were produced and archived. The VAS data consisted of the dwell sounds of nominal spin budgets as well as the higher spin budgets from Meso-A and the Meso-B dwell soundings. The ancillary data consists of surface data and numerical model fields (the Nested Grid Model). Intermediate products were time-interpolated numerical model output files and analyzed surface fields of height, temperature and dew point depression. Final products consisted of VAS retrievals calculated on the MIDAS computer in Washington, D.C. and the forward brightness temperature calculations based on the interpolated numerical model fields from the U.W. McIDAS mainframe. The VAS retrievals were generated every three hours, whereas the forward calculation was completed every six hours. An IBM RISC-6000 was used for local processing as well as communications and data transfer.

A summary of VAS data archived on magnetic cartridges is shown (Table 1). Note that RISOP (rapid imaging) mode which precludes VAS data acquisition lasted for some extended time periods. For non-RISOP days, additional VAS dwell sounds not listed in Table 1 could be obtained via the cassette archive. Lack of retrievals from the MIDAS was due to communication problems to no surface nor model information on the system.

In all, 13 cartridges have been filled consisting of over 200 MB of data. Efforts are underway to make these data a part of the STORM-FEST data Systems Archive.

Table 1. STORM-FEST data archive.

DATE	DAY	IOP (#)	RISOP (time)	DS (area)	MESO-B (area)	Forward Calc.	RETVL (MIDAS)	SFC File	GUESS Analysis	SFC Analysis
92032	01 Feb									
92033	02 Feb					Y				
92034	03 Feb									
92035	04 Feb			Y		Y		Y	Y	Y
92036	05 Feb			Y	Y	Y		Y	Y	Y
92037	06 Feb		21-24Z	Y	Y	Y	Y	Y	Y	Y
92038	07 Feb		21-24Z	Y	Y	Y	Y	Y	Y	Y
92039	08 Feb		00-01Z	Y		Y	Y			Y
92040	09 Feb	3		Y		Y	Y		Y	Y
92041	10 Feb	4	21-24Z	Y	Y	Y	Y	Y	Y	Y
92042	11 Feb	5	00-01Z; 12-24Z	Y		Y		Y	Y	Y
92043	12 Feb	5	00-12Z	Y	Y	Y	Y	Y	Y	Y
92044	13 Feb			Y	Y		Y	Y	Y	Y
92045	14 Feb		12-24Z	Y	Y	Y		Y	Y	Y
92046	15 Feb		00-14Z	Y		Y	Y			Y
92047	16 Feb			Y	Y	Y	Y	Y	Y	Y
92048	17 Feb		00-24Z							
92049	18 Feb		20-24Z	Y	Y	Y	Y	Y	Y	Y
92050	19 Feb	8	21-24Z	Y	Y	Y	Y	Y	Y	Y
92051	20 Feb		00-01Z	Y	Y	Y	Y	Y	Y	Y
92052	21 Feb		22-24Z	Y	Y	Y	Y	Y	Y	Y
92053	22 Feb		00-05Z	Y	Y	Y	Y	Y	Y	Y
92054	23 Feb		12-24Z	Y		Y	Y	Y	Y	Y
92055	24 Feb	11	00-24Z							
92056	25 Feb	12	00-01Z	Y		Y	Y	Y	Y	Y
92057	26 Feb			Y	Y	Y	Y	Y	Y	Y
92058	27 Feb	13		Y	Y	Y	Y	Y	Y	Y
92059	28 Feb			Y	Y	Y	Y	Y	Y	Y
92060	29 Feb			Y		Y	Y	Y	Y	Y
92061	01 Mar	15		Y		Y	Y	Y	Y	Y
92062	02 Mar			Y		Y	Y	Y	Y	Y
92063	03 Mar	16	18-24Z	Y		Y	Y	Y	Y	Y
92064	04 Mar	16	00-24Z							
92065	05 Mar	16	00-02Z	Y		Y	Y	Y	Y	Y
92066	06 Mar			Y		Y		Y	Y	Y
92067	07 Mar			Y		Y		Y	Y	Y
92068	08 Mar	17	12-24Z	Y		Y		Y	Y	Y
92069	09 Mar	17	00-24Z							
92070	10 Mar	18	00-24Z							
92071	11 Mar	19	00-03Z; 12-24Z	Y	Y		Y			
92072	12 Mar	20	00-01Z; 22-24Z	Y	Y	Y	Y	Y	Y	Y
92073	13 Mar		00-02Z; 21-24Z	Y	Y	Y	Y	Y	Y	Y
92074	14 Mar			Y	Y	Y		Y	Y	Y

D. THE SOUTHWEST AREA MONSOON PROJECT (SWAMP). Contributed by Gary S. Wade.

In support of the July-August 1990 SWAMP (SouthWest Area Monsoon Project) field experiment, VAS dwell sound and MSI (Multi-Spectral Image) data were collected over the southwestern US and northwestern Mexico (Wade, 1992). From a number of cases, which involved special flights of the instrumented NOAA P-3 aircraft, the evening of 2-3 August 1990 was selected for study with the VAS data. Sufficient coverage with VAS infrared soundings was anticipated with this case, due to the mostly clear conditions over the SWAMP region. The P-3 flight coverage extended over the extreme northern Gulf of California to examine moisture structure, and then, over southern Arizona to monitor local storms.

Moisture fields were produced from both the MSI data (at 2 hourly intervals from 1801 UTC on the 2nd through 0401 UTC on the 3rd) and the dwell sound data (paired at 2018/2048, 0048/0118, and 0218/0248 UTC). The former quantities were of **total** precipitable water vapor only while the latter products consisted of **two layers** of precipitable water vapor (PW). These moisture sequences are shown in Figures 1 and 2.

In Figure 1, the VAS MSI PW data are presented in an image format, overlaid with contours from the time-interpolated 12 UTC 2 August 1992 NGM numerical model data. Both data sources show very moist values over Texas and very dry values over central northern Mexico. The moist streak extending from the southwest corner of each VAS image appears oriented along the moist ridge of the model data. However, differences also exist. The strong moisture gradient from southern California into northwestern Mexico, just north of the Gulf of California, progresses eastward in the VAS data but remains stationary in the model-derived fields. In addition, the moist maximum across Baja California and the Gulf in the numerical model data contrasts with the dry values from the VAS data over central and southern Baja.

The very moist pocket over Mexico, just east of the Gulf of California, persisted throughout the period. The decay of the convection in that region from 1800 through 2200 UTC remained puzzling, as heat and moisture appeared to be abundant. Lack of in-situ observations over most of the Mexican region prevented actual verification of the VAS patterns.

In Figure 2, the VAS dwell sound PW data are shown for two layers: surface to 0.84 sigma and above 0.84 sigma, where sigma is the ratio of the pressure of the level to the surface pressure. The top panels show the gridded upper level PW fields for each dwell sound period, displayed over the observed VAS 6.7 micrometer water vapor imagery, while the bottom panels show the lower layer patterns over the VAS 11 micrometer window channel. The maximum (moist) values in the lower layer developed over the Gulf. The drying along the California/Arizona border was also observed in the MSI data. The upper layer maximum (15+ mm), which moved east southeastward along and south of the southern Arizona border, seemed to follow the 500 hPa trough over the region. The narrow moist band from the southwest noted in the MSI imagery is not well supported by the full soundings. It appears that this is a situation where the MSI product has been unduly influenced by the first guess (the NMC forecast contoured in Fig. 1). This result is corroborated by a more detailed study presented in a companion paper in this report. With this

exception, reasonable and interesting moisture patterns have been observed in current VAS derived PW imagery over the data sparse Southwest region. Lack of in-situ data has prevented substantial verification; nonetheless, features on the mesoscale have been noted and further investigation is needed.

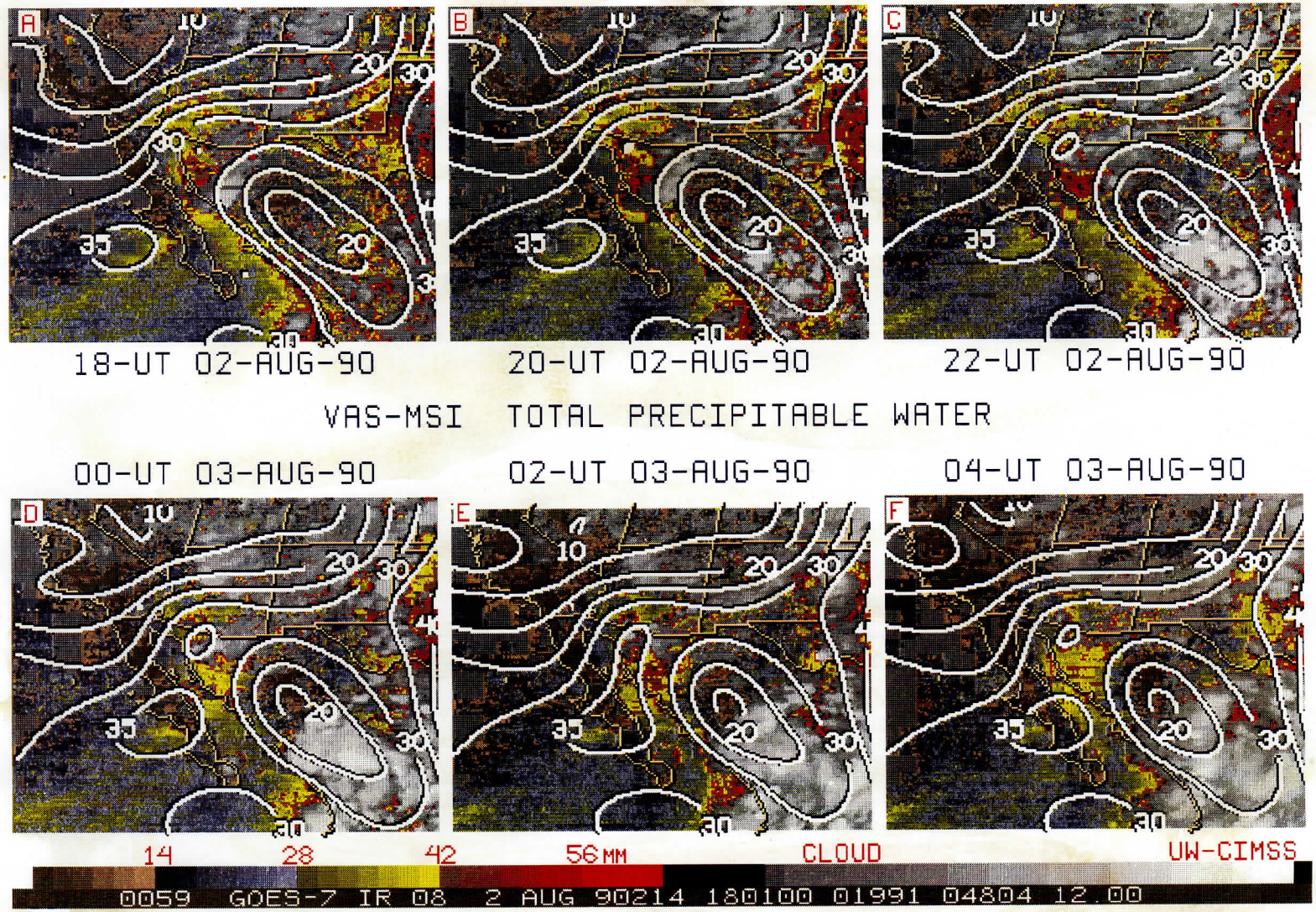

Figure 1. VAS MSI PW data overlaid with contours from the time-interpolated 12 UTC 2 August 1992 NGM numerical model data.

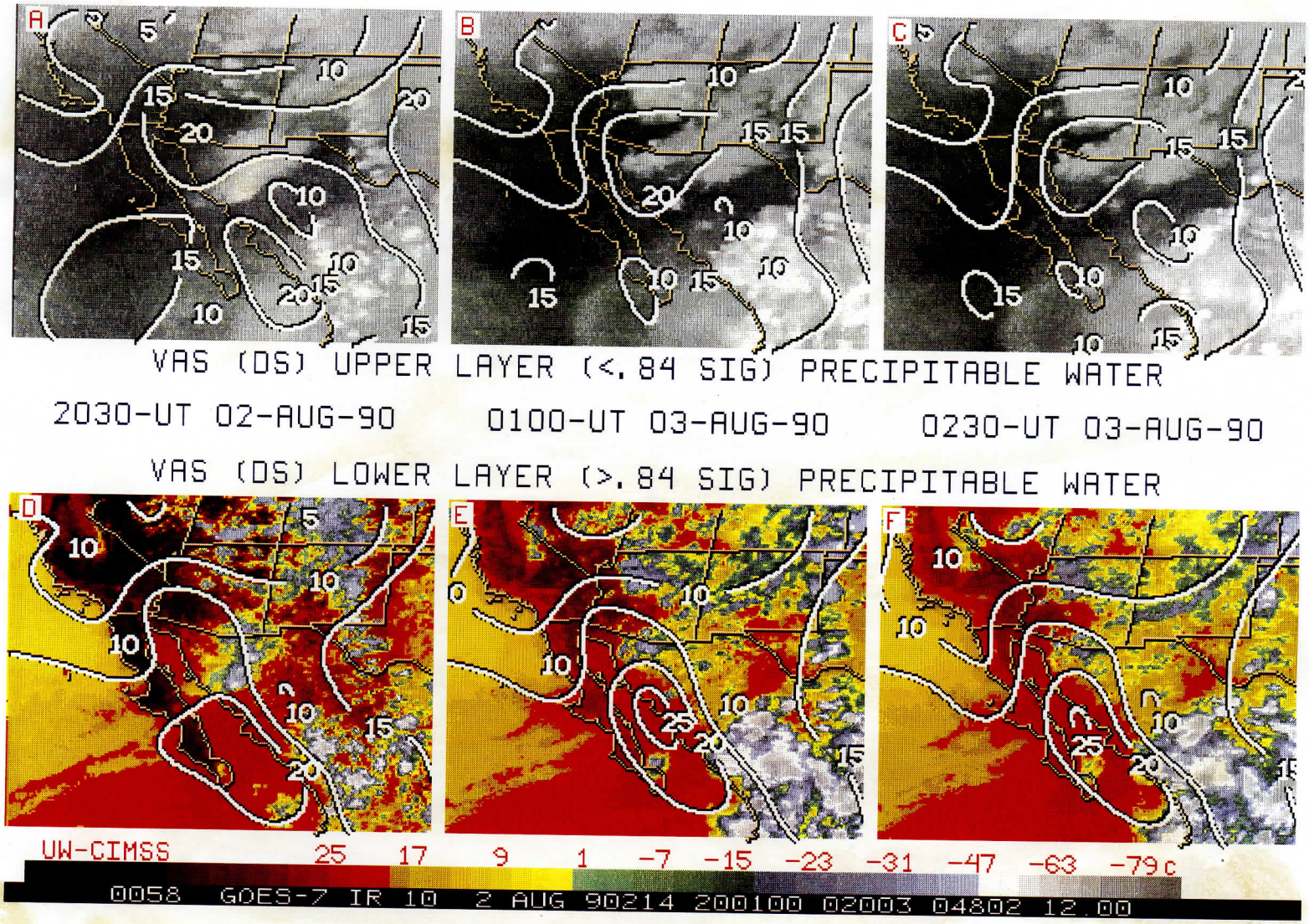

Figure 2. The VAS dwell sound PW data for two layers. The surface to 0.84 sigma is portrayed on top, and the layer above 0.84 sigma is portrayed in the lower panels.

E. THE CIMSS REGIONAL ASSIMILATION SYSTEM. Contribution by Robert M. Aune.

The Analysis/Forecast System

The CIMSS Regional Assimilation System (CRAS) was configured for STORM-FEST in January, 1992. The system (referred to as the opsrun) was executed automatically every 12 hours and produced a 36 hour forecast. Execution of the complete opsrun, including the Analysis/Preprocessing Subsystem, the Model Assimilation Subsystem, and the Postprocessor Subsystem took approximately 2.5 hours of wall time on an IBM Series 6000 RISC Model 550. Three and four dimensional data sets were produced as part of the opsrun for viewing on various display platforms. Forecast data sets were also transferred to McIDAS for viewing by STORM-FEST personnel.

The STORM-FEST Opsrun

The opsrun analysis was performed on a limited area domain with a horizontal resolution of 80 km. The vertical resolution is 50 hPa., 20 levels are used starting at 1000 hPa. The analysis is performed using successive corrections with mass-momentum coupling provided by a variational blend of optional velocity components (gradient, geostrophic, non-divergent or real winds) with analyzed geopotential heights (Seaman, et al., 1977). Input data sets include significant and mandatory rawinsondes which were validated against a background guess from the RAFS analysis. Data quality assignments are made using background field checks and neighborhood checks using statistical interpolation parameters describing the variances and correlation functions of background field errors and observational errors. After the analysis is complete a preprocessor is run to interpolate the analyzed fields from pressure surfaces to a user specified sigma vertical coordinate. Further quality checks are made to eliminate errors introduced by the vertical interpolation.

The forecast subsystem of the CRAS, known as the CIMSS Sub-Synoptic Model (SSM), consists of a state-of-the-art primitive equation model developed by Leslie, et al., 1985. The forecast is performed on the same horizontal domain as the analysis. An Arakawa C grid is used in the model. Twenty sigma levels are used in the vertical. The model uses a semi-implicit time integration scheme and a flux form of the equations. Physical parameterizations include: vertical diffusion, cumulus parameterization, large scale precipitation with evaporation, stability dependent bulk planetary boundary layer (PBL) with eddy diffusivities a function of bulk Richardson number, and a surface heat budget with a prognostic equation for surface temperature. Initial imbalances in the initial fields are reduced using a vertical normal mode initialization (Bourke and McGregor, 1983).

Model fields were output every 2 hours, post processed onto pressure surfaces, and viewed using PC/DOS and UNIX/RISC software packages developed at CIMSS. A software package to generate objective verification statistics has, more recently, been introduced as part of the opsrun. Verification statistics, not available at this time, will be used to tune model parameters in the future. Subjective

verification is conducted using the available display software. Figure 1 shows the 24 hour accumulated precipitation (mm.) from a forecast that commenced on 08 March 1992 at 12 UTC. For comparison, data from the observation network are also plotted (underscored). Area coverage of the predicted precipitation is quite good, although amounts tend to be over-predicted. Four-dimensional data sets were produced for VIS-5D (Visualization of 5-Dimensional Data sets), a software system that allows a user to interactively explore atmospheric parameters as 4-dimensional gridded data sets (Hibbard and Santek, 1990). Figure 2 shows step 13 from a 19 step VIS-5D data set depicting the 24 hour forecasted 45 m/s isotach surface (red), liquid cloud (gray), ice cloud (light gray), and falling precipitation (blue) valid for 9 March 1992 at 00 UTC. This frame is valid at the mid point of the precipitation accumulation period shown in Fig. 1. The domain extends between 74W to 128W and 20N to 56N and from the surface to 12 km. A developing low pressure system over western Kansas is producing precipitation in Nebraska, Kansas, Oklahoma, and Texas.

A major goal of the Assimilation Group at CIMSS is to be able to run the CRAS in real-time, producing control forecasts and assimilation forecasts simultaneously to assess the impact of various data sources, in particular, remotely sensed data from satellites. Since the opsrun was implemented on February 1 1992 a 96% completion rate has been achieved. All failures were a result of the non-receipt of initial data. All data required to reproduce a particular forecast are archived on 1/4 inch tape.

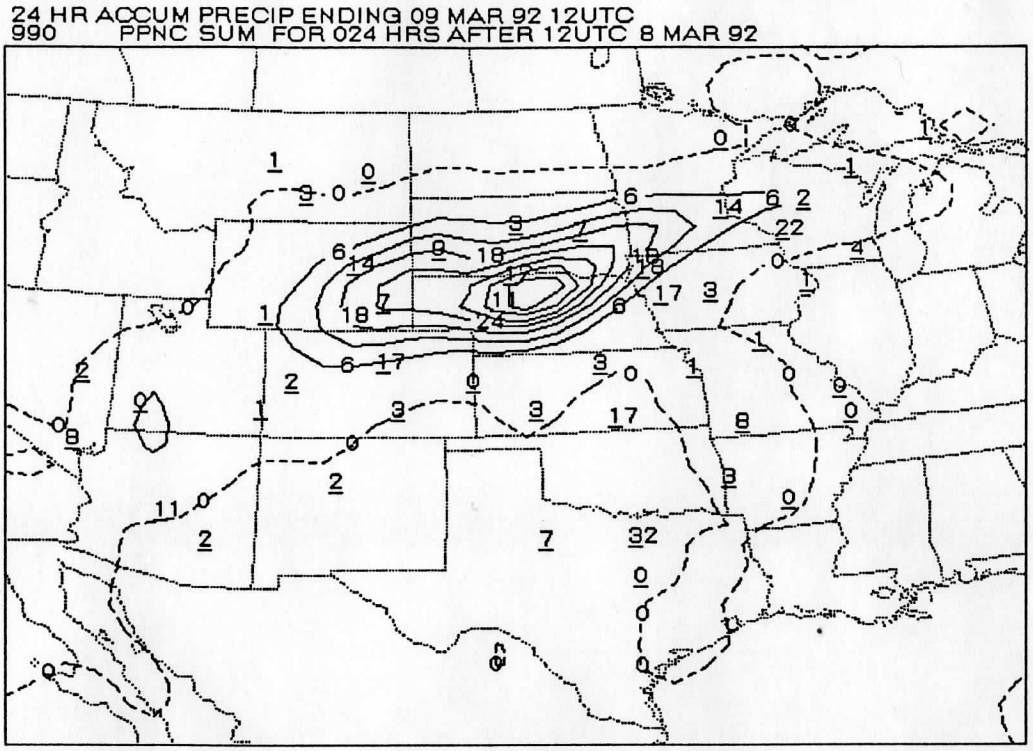

Fig. 1. 24 hr. accumulated precipitation (mm.) from a forecast that commenced on 08 March 1992 at 12 UTC. Observed 24 hr. accumulations are plotted with an underscore.

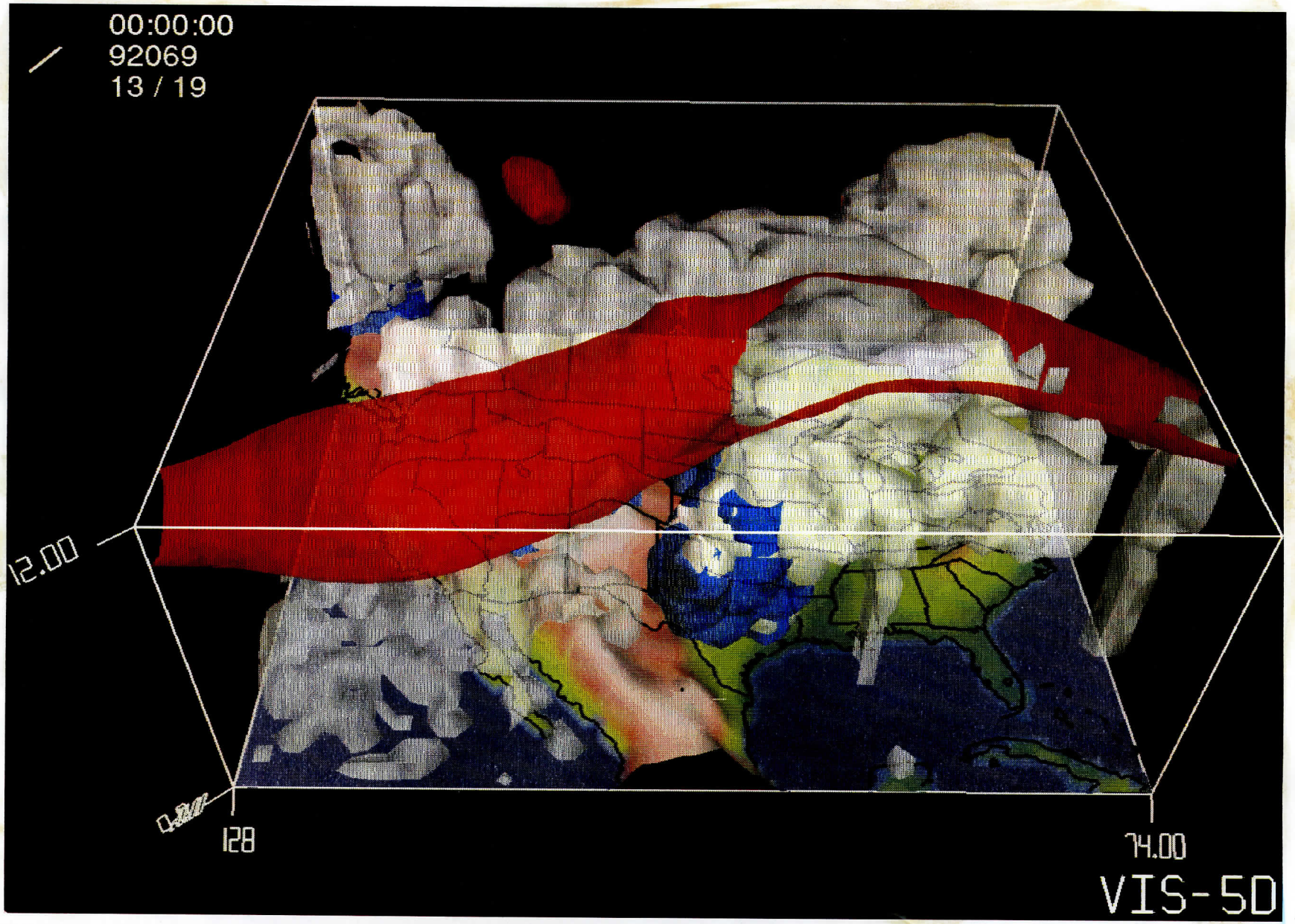

Figure 2. Step 13 from a 19 step VIS-5D data set depicting the 24 hr. forecast fields of the 45 m/s isotach field (red), liquid cloud (gray), ice cloud (light gray), and falling precipitation (blue) valid 9 March 1992 at 00 UTC.

F. DATA ASSIMILATION OF DIABATIC HEATING AND CLOUD LIQUID WATER.

Contribution by Xiaohua Wu.

This report summarizes work completed on the numerical processing of diabatic initialization and cloud water initial specification on the CIMSS Sub-Synoptic Model (SSM) and their impact on model forecasting. The work includes the analysis of dynamic balance induced by diabatic initialization; the development of a diagnostic method with which to specify initial cloud water distribution; and a numerical precipitation forecasting test using the cloud water diagnostic method in conjunction with diabatic initialization. A detailed description of the technique can be found in Wu, (1991).

The current work tests the application of diabatic initialization in order to analyze the dynamic balance induced by diabatic VMI, since it is important to know whether diabatic VMI is able to achieve dynamic balance (Kasahara, et al., 1992). For this study, the variations of vertical velocity and precipitation based on adiabatic and diabatic initialization with different modes are compared, using the initial fields from a "control run" which is a 12 hour forecast started from 00z, March 13 of 1991. If a balance condition induced by a certain initialization is obtainable, the variations of vertical velocity after the initialization should be consistent with that of the control run. Fig. 1 shows the time variation of vertical velocity at selected grid points (either raining or clear at initial time) on the 0.51 sigma level (close to 550 hPa) based on adiabatic and diabatic initialization. In each figure, the initialization is performed at the thirty-sixth time step plotted. (12 hrs.). Comparing the vertical velocity of the control run shows that the performance of diabatic initialization is almost the same as that of the adiabatic mode and that of the control mode. The damping of vertical velocity is more obvious as the initialized total modes increase to larger than 3 in adiabatic initialization. However, diabatic initialization with three and four modes can still retain vertical velocity close to those of one control run. When the initialized total modes are larger than 5, forecasts become unstable for both adiabatic and diabatic initialization. This implies that the balance condition of VMI for higher inner modes larger than 5 is not achievable. Corresponding to Fig. 1, Fig. 2 shows the variations of precipitation on those same grid points. The changes of precipitation have the same characteristics as the variations of vertical velocity for both adiabatic and diabatic initialization.

The test of dynamic balance induced by diabatic initialization indicates (quite naturally) that adiabatic initialization is unable to generate the divergent circulation which are diabaticly driven (as estimated in control forecast). With noiseless diabatic heating rates, diabatic initialization can generate divergent circulation which are consistent with the latent heating sources. A main feature to note is that diabatic initialization seems effective only if some of the higher vertical modes (larger than 3) are initialized. In one mode corresponding to the model's equivalent depth (around 100m) the dynamic conditions of VMI are no longer met. The determination of this threshold mode depends on the mean thermal structure of forecast model. For SSM, it is mode 5.

Cloud water initialization for this study seeks to specify the initial cloud water distribution and to

modify it based on clouds observed by satellite (Diak, et al., 1992). The method involves four steps. The first step is to diagnose the cloud "base" level obtained as follows. After interpolating the "satellite-inferred" observed cloud top height and total amount of cloud water into SSM grids, the vertical gradient of relative humidity (RH) is calculated from "satellite" observed cloud top level downwards. If the change of RH in a certain layer is over 10% per 100 hPa., then the lower level of this layer is defined as the cloud "base". The second step is using a quadratic regressive equation to predict the level of maximum cloud water distribution. The regressive coefficients are statistically obtained from several hundred cloud water vertical profiles forecasted by the SSM. The variables used in the regression equation are total cloud water, cloud top pressure, cloud base pressure, pressure of maximum upward vertical velocity (if it is in the cloud), and the maximum vertical velocity value. The third step is to build the cloud water profile which is constrained by the amount of total cloud water accumulated vertically. Based on the level of predicted maximum cloud water distribution, the cloud water profile may be specified. In a parabolic distribution the maximum cloud water is in the middle part of the cloud. For a Rayleigh distribution the maximum cloud water is in the upper or lower part of the cloud. The final step is to modify the mixing ratio in the cloudy area to make the initial moisture fields consistent with the existing clouds. Fig. 3 shows the comparison of vertical cloud water distributions forecast by SSM and those diagnosed by the method described above for selected grid points.

Using the cloud water diagnostic method in conjunction with the diabatic initialization procedure, the spin up characteristics of precipitation forecasting with a simulated "synoptic" case were tested. For this experiment, a set of vertical soundings of u, v, T and q is extracted from the control forecast experiment at every 400 km in both x and y directions to simulate a rawinsonde observing network. The simulated total cloud water amount is obtained from the control forecast at each 80 km. interval in both x and y directions (an interval appropriate to satellite sounding). Fig. 4 shows the precipitation of this forecasting experiment. Since the application of diabatic VMI alone does not alter the initial moisture distribution, the initial precipitation is still very deficient, even though the initial vertical velocity fields are diabatically consistent with the latent heating sources. However, application of initial cloud water specification, together with diabatic VMI is seen to improve the precipitation spin up problem because of its ability to modify the initial moisture distribution and diagnose the existing clouds.

The expansion of the application of diabatic initialization and initial cloud water specification, using realistic estimates of satellite derived moisture and cloud liquid water, will be tested further in this study.

Fig. 1 Comparisons of vertical velocity on sigma=0.51 (p=550 hPa.) at various grid points. (a), (b), (c) are raining points corresponding to (31,34), (30,35) and (36,34). (d) is (25,20), a clear area point.

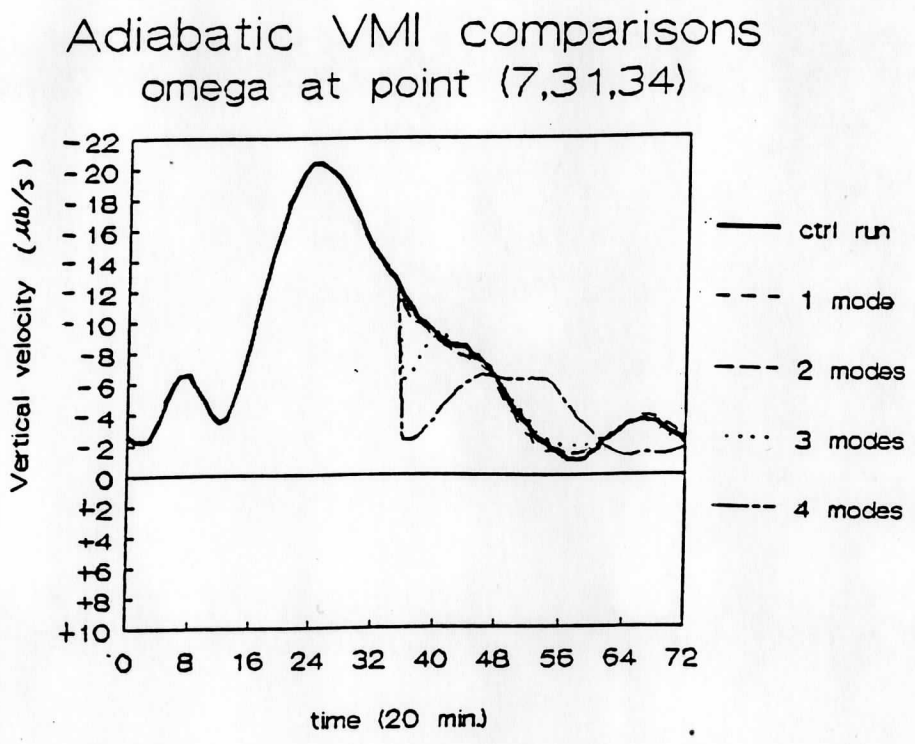

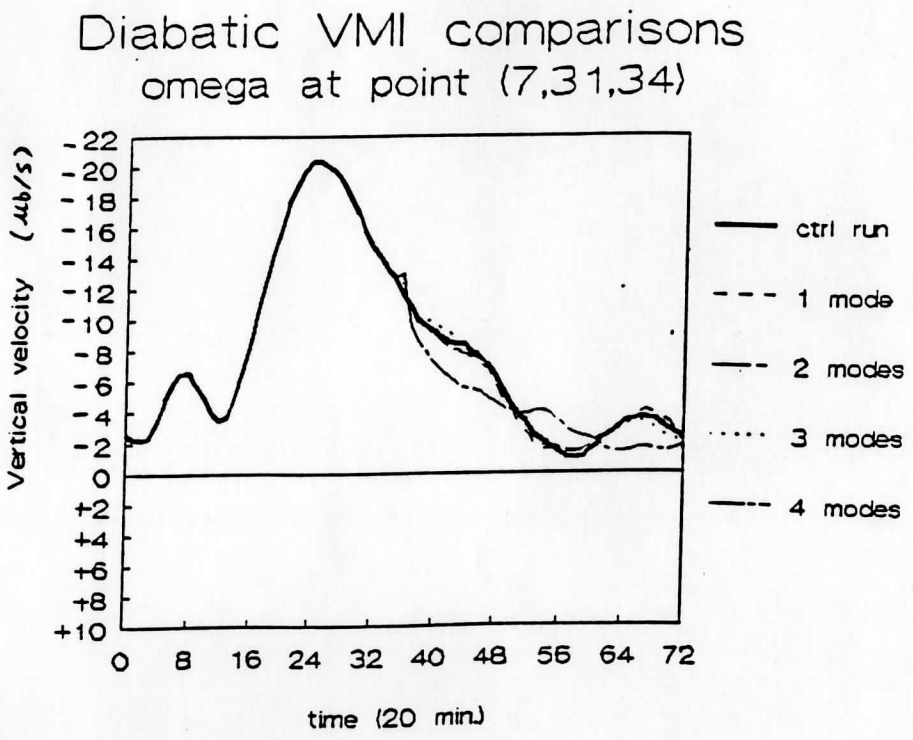

(a)

ig 1

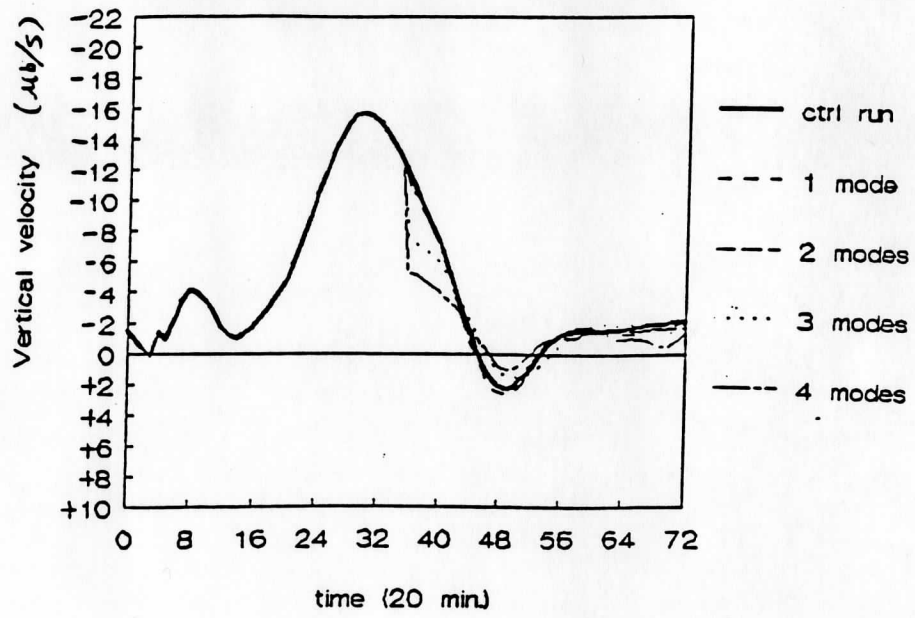
Adiabatic VMI comparisons
omega at point (7,30,35)
Vertical velocity (μb/s)
-22
-20
-18
-16
-14
-12
-10
-8
-6
-4
-2
0
+2
+4
+6
+8
+10
0 8 16 24 32 40 48 56 64 72
time (20 min)
ctrl run
1 mode
2 modes
3 modes
4 modes

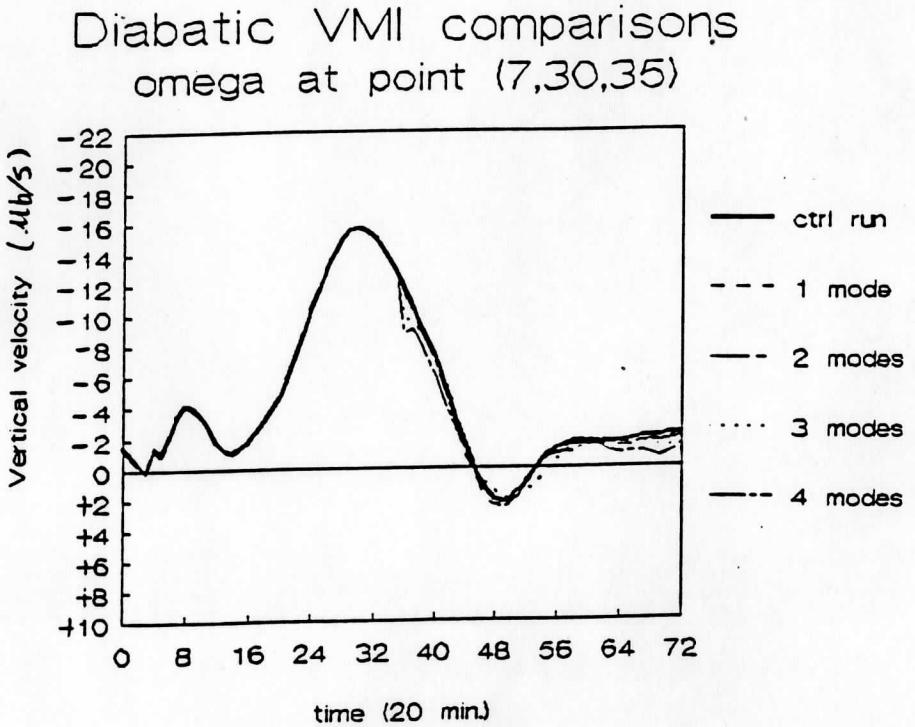
Diabatic VMI comparisons
omega at point (7,30,35)
Vertical velocity (μb/s)
-22
-20
-18
-16
-14
-12
-10
-8
-6
-4
-2
0
+2
+4
+6
+8
+10
0 8 16 24 32 40 48 56 64 72
time (20 min)
ctrl run
1 mode
2 modes
3 modes
4 modes

- (b)

Fig. 1

Adiabatic VMI comparisons
omega at point (7,36,34)

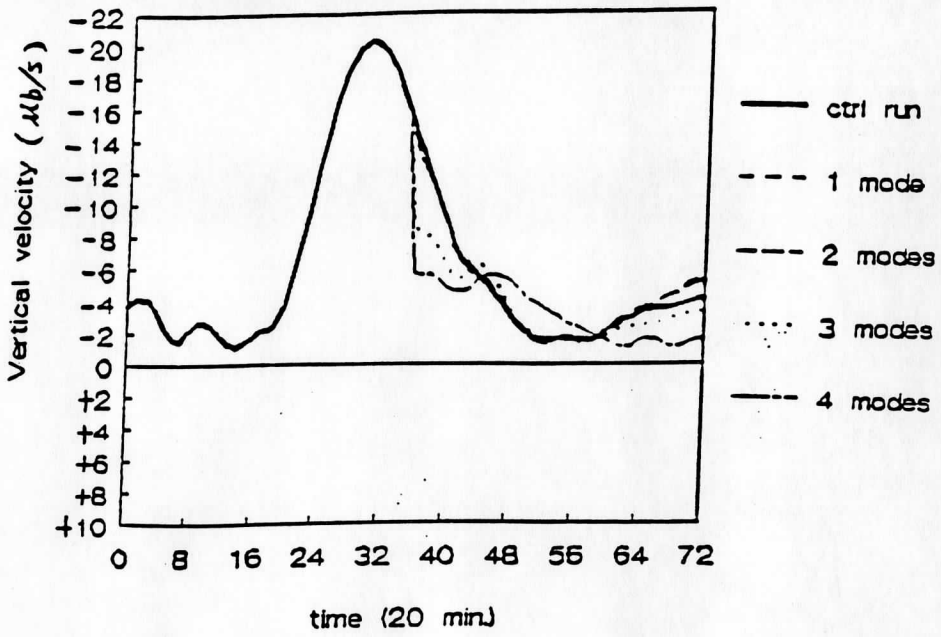

Diabatic VMI comparisons
omega at point (7,36,34)

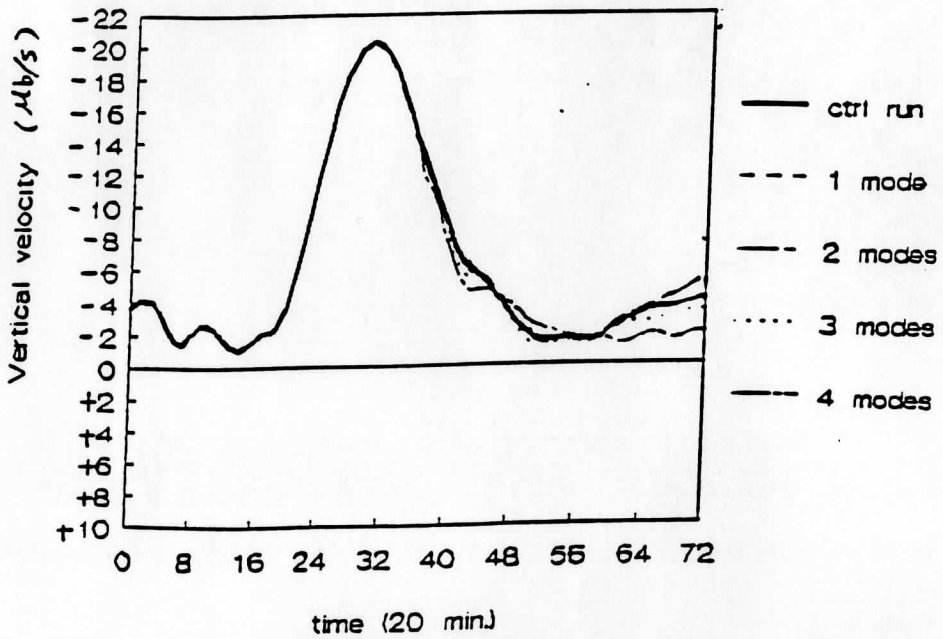

(C)

Adiabatic VMI comparisons
omega at point (7,25,20)

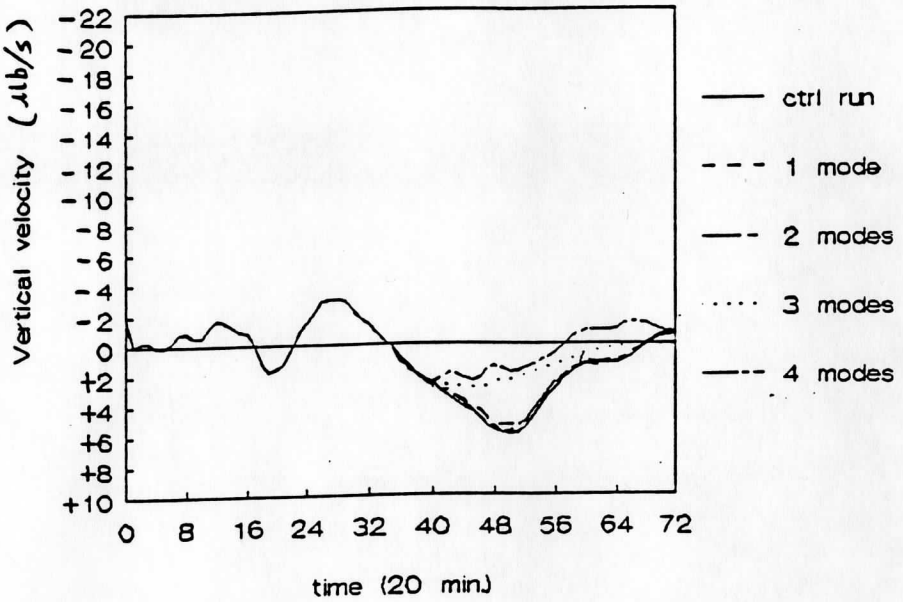

Diabatic VMI comparisons
omega at point (7,25,20)

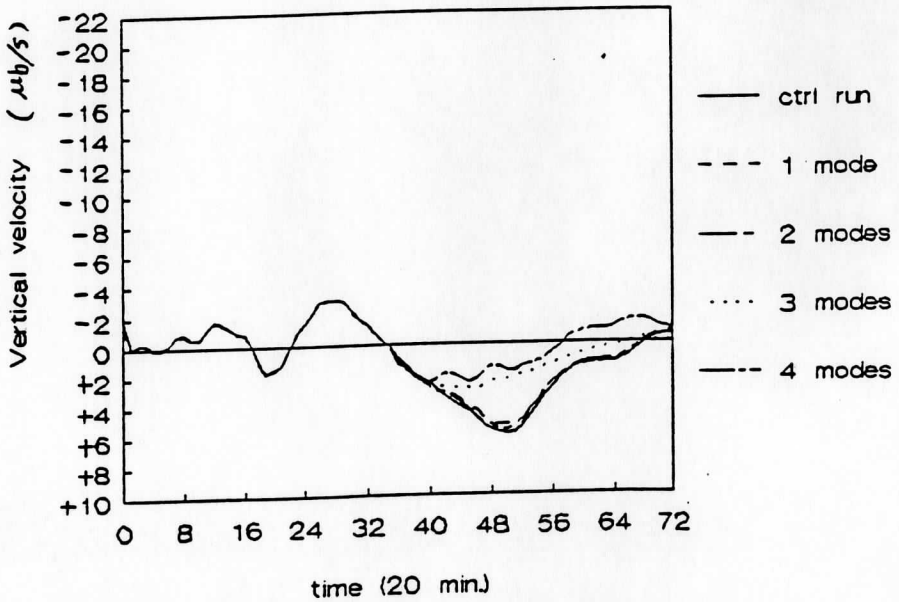

(d)

ig 1

Fig.2 Comparisons of precipitation at the grid points same to Fig.1

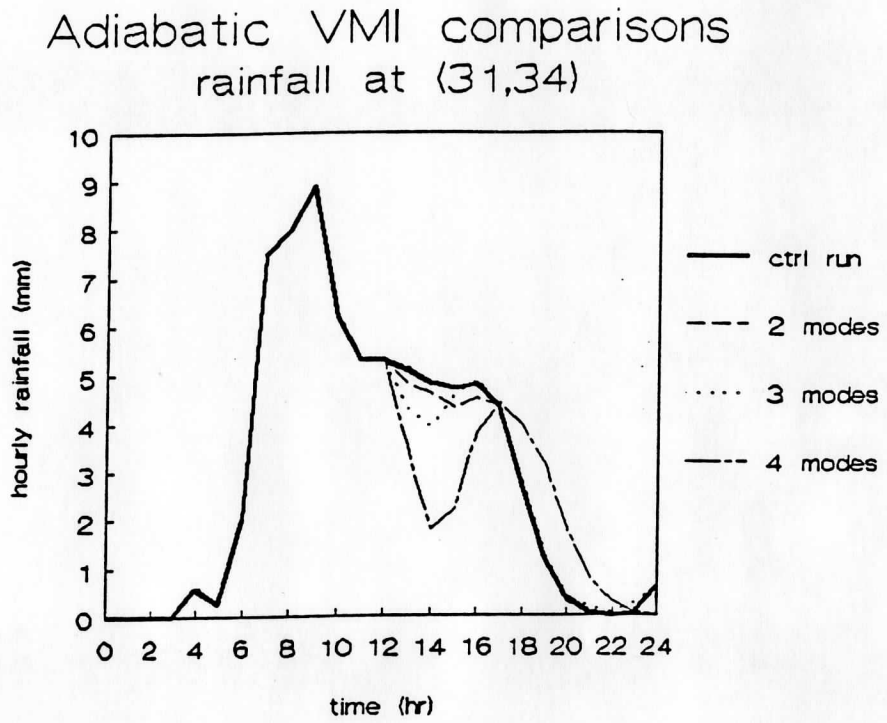

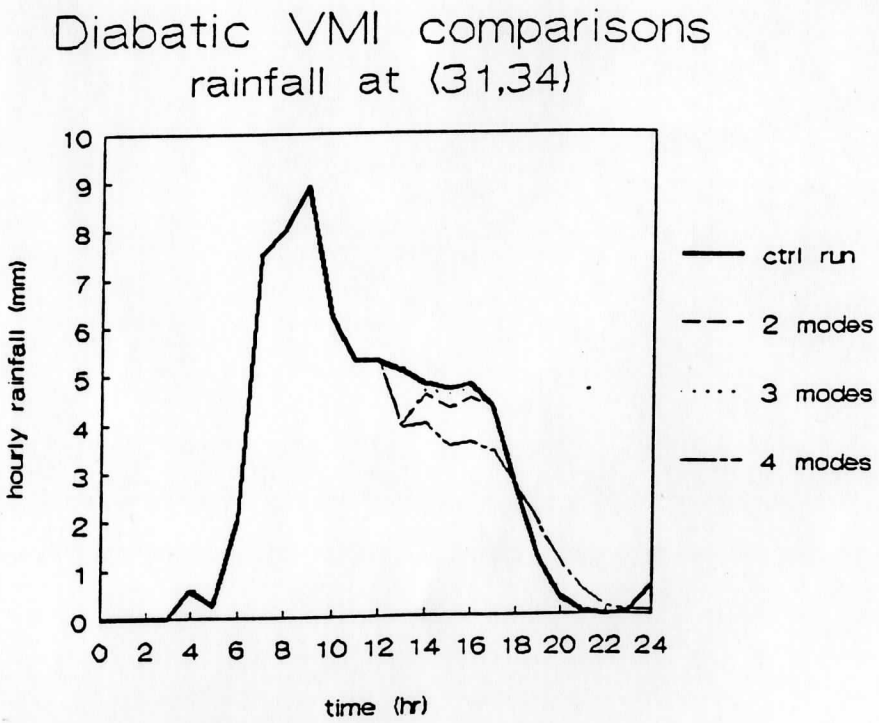

(a)

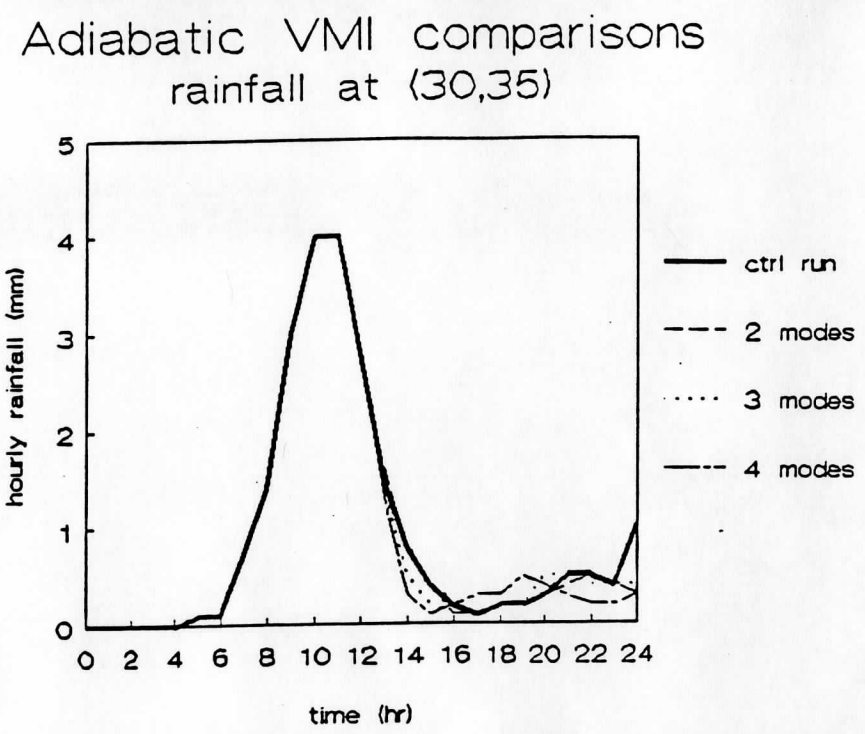
Adiabatic VMI comparisons
rainfall at (30,35)
hourly rainfall (mm)
0
1
2
3
4
5
0 2 4 6 8 10 12 14 16 18 20 22 24
time (hr)
ctrl run
2 modes
3 modes
4 modes

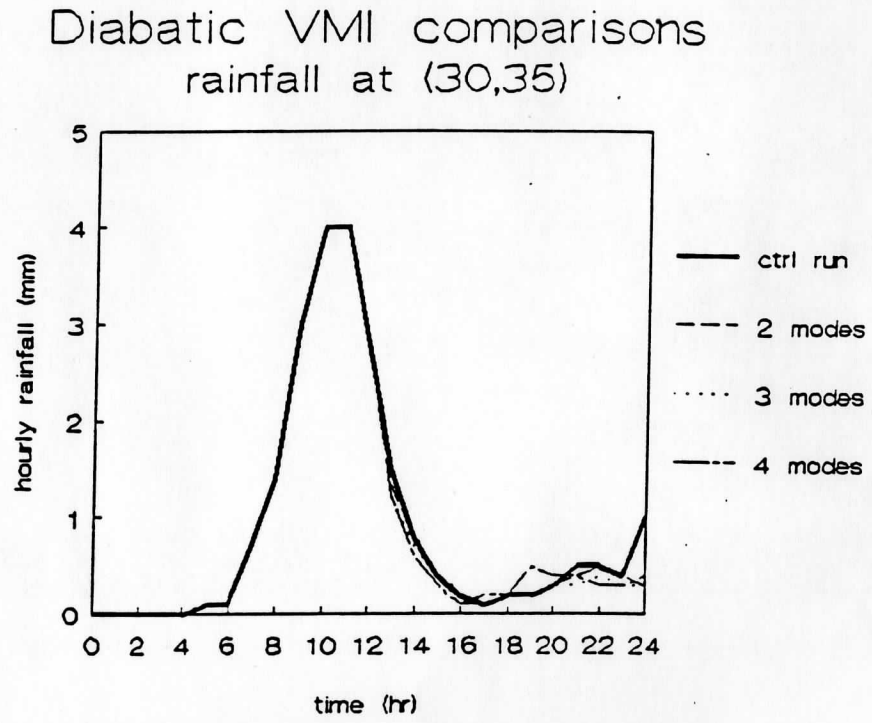
Diabatic VMI comparisons
rainfall at (30,35)
hourly rainfall (mm)
0
1
2
3
4
5
0 2 4 6 8 10 12 14 16 18 20 22 24
time (hr)
ctrl run
2 modes
3 modes
4 modes

(b)

Fig 2

Adiabatic VMI comparisons
rainfall at (36,34)

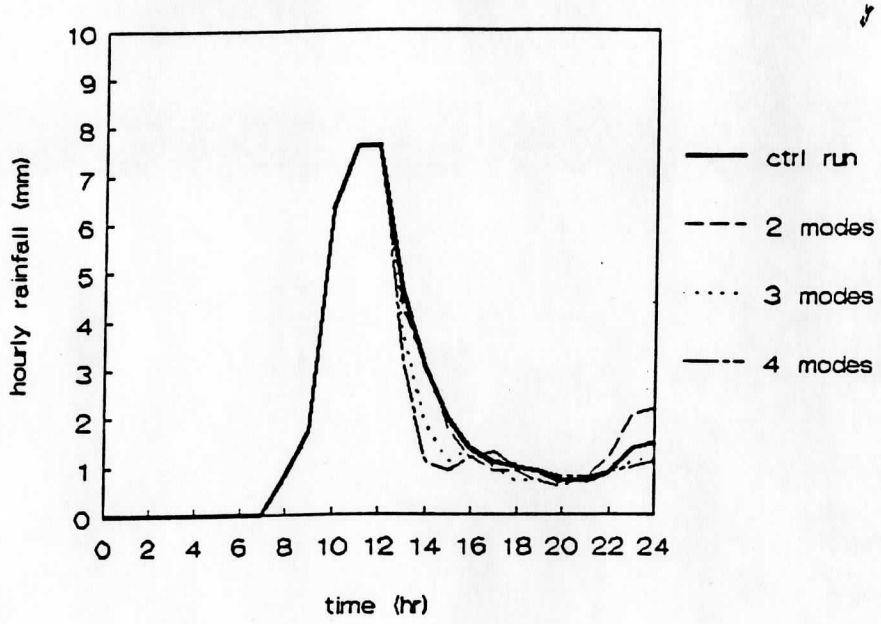

Diabatic VMI comparisons
rainfall at (36,34)

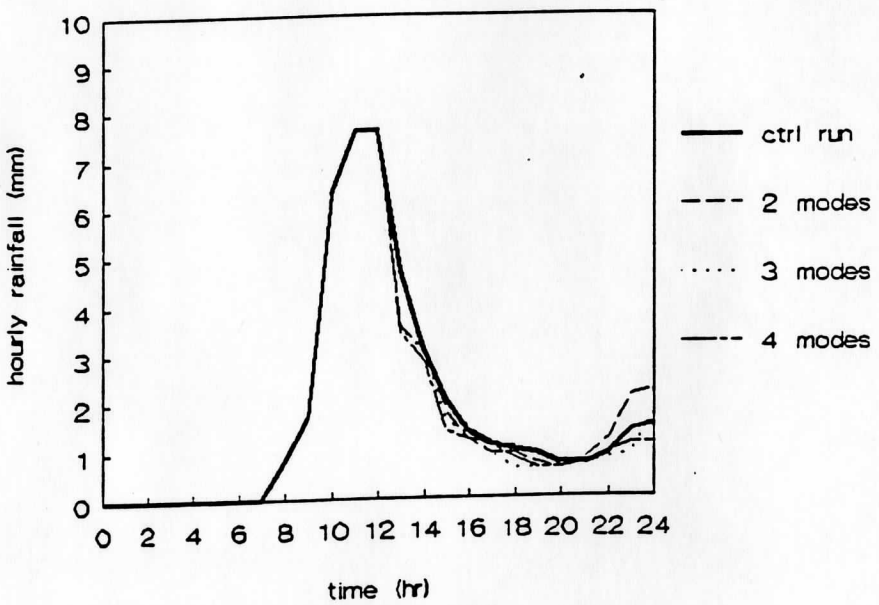

(C)

Fig 2

Fig. 3 Cloud water (CW) profiles. The solid line represents CW profile for the control run and dash line is the specified CW profiles for the diagnostic method.

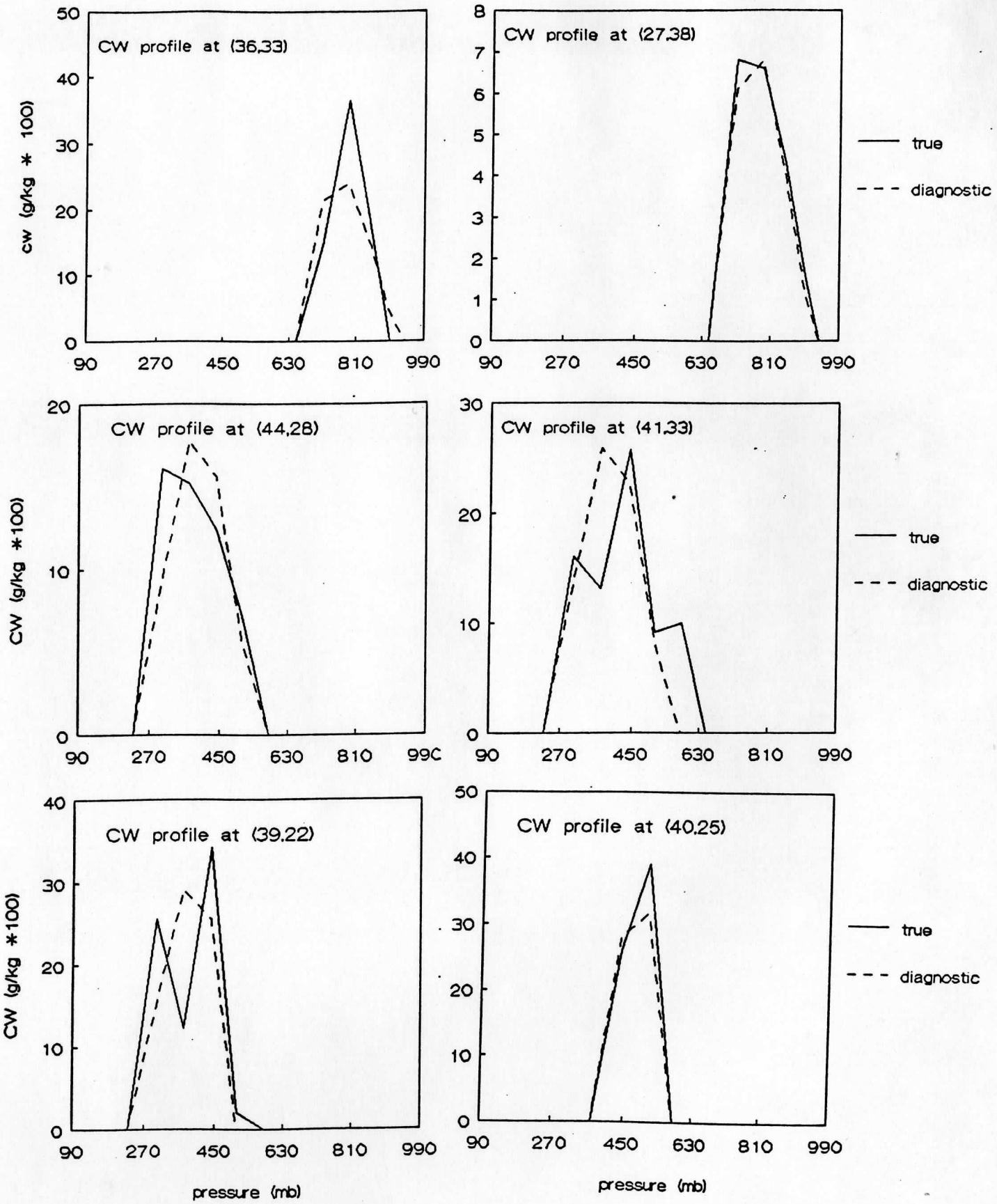

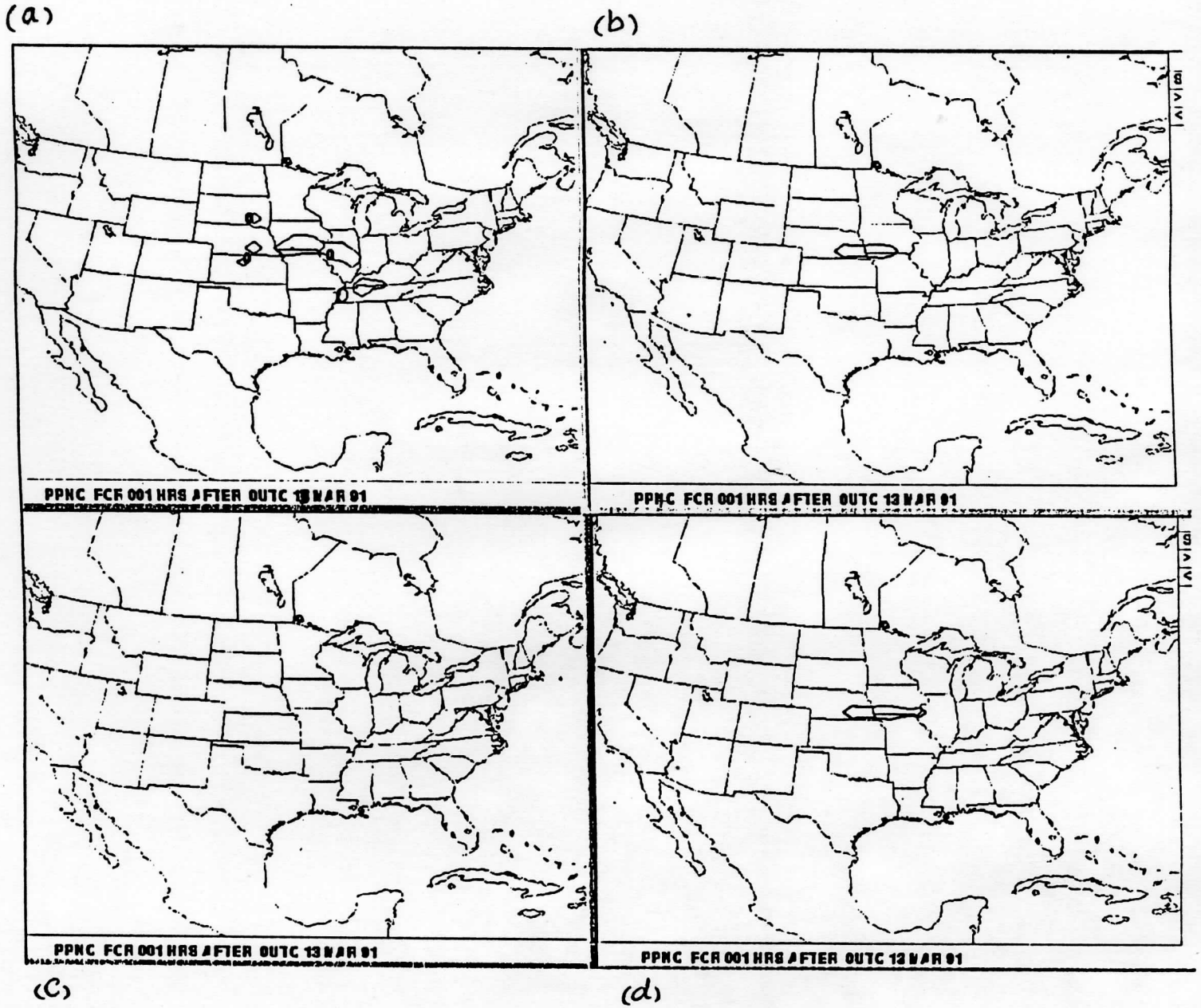

Fig. 4 Precipitation forecasted by SSM with diabatic initialization and initial cloud water specification at one (Fig. 4.1), two (Fig. 4.2) and four hour (Fig. 4.3) point of the model run. In this case (a) is control run, (b) is the diabatic VMI and initial CW specification, (c) is the adiabatic initialization and no initial CW specification and (d) is the adiabatic VMI and initial CW specification.

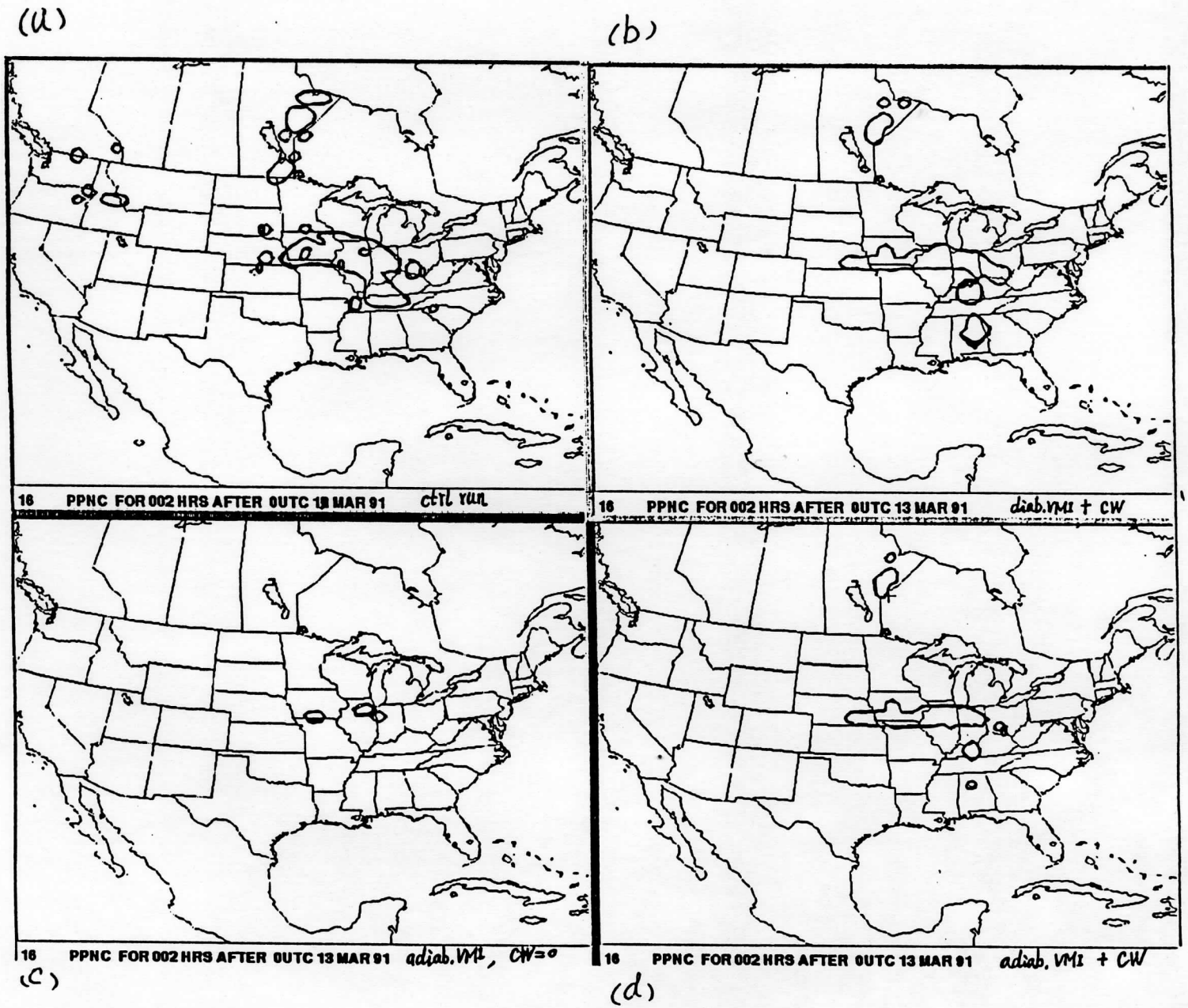
(a)
(b)
16 PPNC FOR 002 HRS AFTER 0UTC 13 MAR 91 ctrl run
16 PPNC FOR 002 HRS AFTER 0UTC 13 MAR 91 diab. VMI + CW
16 PPNC FOR 002 HRS AFTER 0UTC 13 MAR 91 adiab. VMI, CW=0
16 PPNC FOR 002 HRS AFTER 0UTC 13 MAR 91 adiab. VMI + CW
(c)
(d)

Fig. 4.2

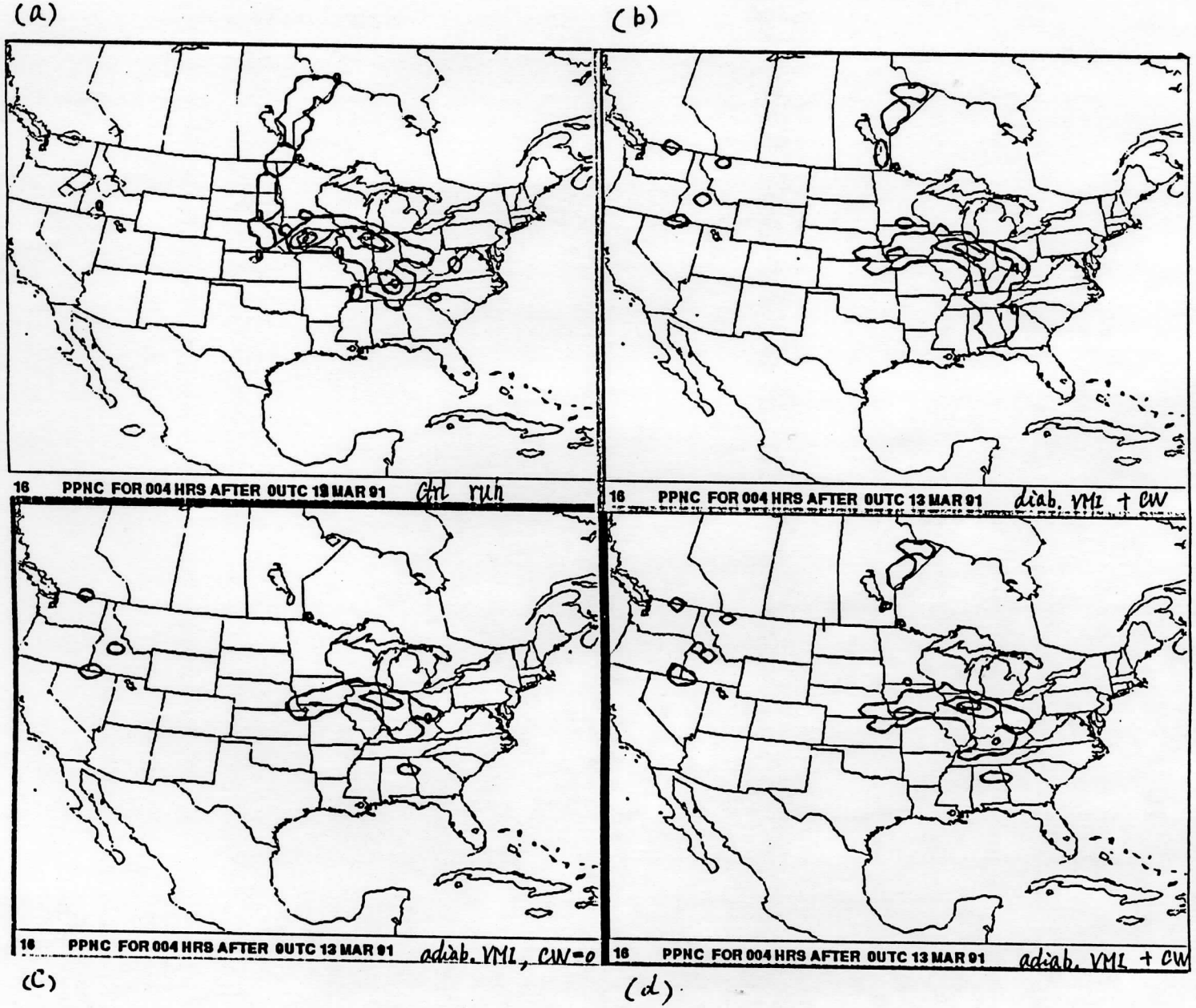
(a)
(b)
16 PPNC FOR 004 HRS AFTER 0UTC 13 MAR 91 Ctrl run
16 PPNC FOR 004 HRS AFTER 0UTC 13 MAR 91 diab. VMI + CW
16 PPNC FOR 004 HRS AFTER 0UTC 13 MAR 91 adiab. VMI, CW=0
16 PPNC FOR 004 HRS AFTER 0UTC 13 MAR 91 adiab. VMI + CW
(c)
(d)

Fig. 4.3

G. EFFECTIVENESS ON THE SURFACE AIR TEMPERATURE MODEL USED IN THE DETERMINATION OF CLEAR RADIANCES FOR VAS. Contribution by Anthony J. Schreiner and Christopher M. Hayden.

Introduction

VAS dwell sounds and surface observations do not typically occur simultaneously. The importance of these mutually exclusive events can be very critical during the periods just before and after sunrise and sunset, when analyzed fields of surface temperature are used to determine whether a VAS field of view (fov) is either clear or cloudy. A simple diurnal surface temperature model developed to compensate for this discrepancy was tested.

Theory

The surface tendency model estimates the hourly change in the surface air temperature as well as the difference between surface air and surface skin temperatures. The tendencies are calculated from a very simple model of solar heating which requires only the date, hour, latitude, longitude, and surface dew point depression.

Surface tendencies are based on the cosine of the solar zenith angle. The maximum amplitude of the heating is a function of a defined constant, and is modulated by the albedo and the surface dew point depression. In principal, the smaller the albedo the greater the heating, and the smaller the dew point depression the less the heating.

From the calculated sunrise and sunset, the time of local noon is obtained which permits the calculation of the maximum solar zenith angle. The noon zenith angle allows definition of the maximum heating. Using a very simple concept of energy conservation such that total solar heating is balanced by long wave cooling over the day, an hourly cooling rate is defined. The heating is assumed to lag the sun cycle by a fixed amount. If desired the lag can be modified.

The surface air temperature tendency is derived from the difference of heating at two times. The first time is the observation time minus the lag and the second time is defined as a half hour earlier. There is an intentional discontinuity at either sunrise or sunset, when the heating jumps from the fixed cooling rate to zero or vice versa. The discontinuity is smoothed by averaging the cosine heating and fixed cooling rate during the bracketed time periods.

The skin-air temperature difference calculation uses the same technique, but instead of determining tendencies, the actual values of heating are generated. From lagged sunrise to sunset, the difference is a fixed fraction. During the lagged night the difference is accumulated. The general trend of the model is to have cosine positive values from the fixed lag time past dawn until the fixed lag time past sunset. During the lagged night the negative difference increases linearly with time.

There are a number of shortcomings to the model. Principally they are:

- The concept of an energy balance to specify the nocturnal cooling rate is certainly flawed by the fact that the current dew point depression is used to specify the "balance" for the entire day. However, it is not obvious how this can be improved in a simple way.
- There is no requirement to use a constant albedo, but this is currently the practice (value=0.23). With more sophisticated processing of the satellite data the albedo should become dynamic.
- A surface skin - air model which does not take into account the boundary layer wind is almost mindlessly naive. Unfortunately, the current GOES software does not carry analyses of surface wind. Plans exist to correct this deficiency.

Discussion

To observe the variations that may occur at one location for three different seasons and to identify the characteristics of the diurnal temperature curve for other than completely clear situations a set (Figures 1-3) of graphs were generated. Strong cooling is observed in the afternoon-sunset-early evening period for all three figures. In the fall (figure 3) case the maximum amount of heating is greater than for the summer case (figure 2). There are two reasons for this. First, the dew point depression does not exceed 4.0 C until after 16 UTC in the summer case. Second, cloudy conditions occur throughout the day in the summer situation in the form of scattered to broken low level from 00 UTC through 17 UTC and scattered low and cirrus level clouds from 18 UTC through 23 UTC. In all cases, with the possible exception of the summer case, the calculated amplitude of maximum heating is too great. In general, the slopes of the tendencies appear to coincide well even in these somewhat cloudy cases even though the calculated and observed values are not of the same sign, much less equal. The exception to this is the period after sunset when the observed cooling rates are not nearly as severe as the calculated values for all lag times and maximum heating values.

Summary

Early results from this investigation have shown that: (1) Calculated values of surface temperature begin to cool too early and fast during the late afternoon, sunset, and early evening period. To this point it has been impossible to correct for this deficiency. (2) The model does not begin heating fast enough during the period just after sunrise. Although this can be significantly compensated for by adjusting the lag term.

Some advantages are: (1) Even though the value of the cooling rate is higher for the calculated hourly surface temperature change, the rate of the cooling rates (the slopes of the curves) is similar for both the observed and the calculated throughout the late afternoon and into the evening. The exception to this is the period after sunset where the model depicts significantly cooler values than observed. (2) Hourly changes through the nighttime periods for all days show the calculated comparing well with observed.

In general, the model works quite satisfactory, given its simplicity and minimal number of input parameters. The largest problems arise in the late afternoon-sunset-early evening period. Even there the

slope of the surface temperature tendencies are the same as observed values, except during the early evening period. Of interest is that the dew point depression remains large during the late hours of sunlight for as much as one to two hours after sunset. This may be a contributing factor in the calculated hourly temperature changes demonstrating a much faster falling off from the daily maximum than the observed.

For all its simplicity and inherent error, the model clearly improves the cloud identification properties of the GOES retrieval algorithm, and has been incorporated operationally. Further examination of this model for different terrain types and various local climatic conditions are required. Work in this area will continue during the current contract year.

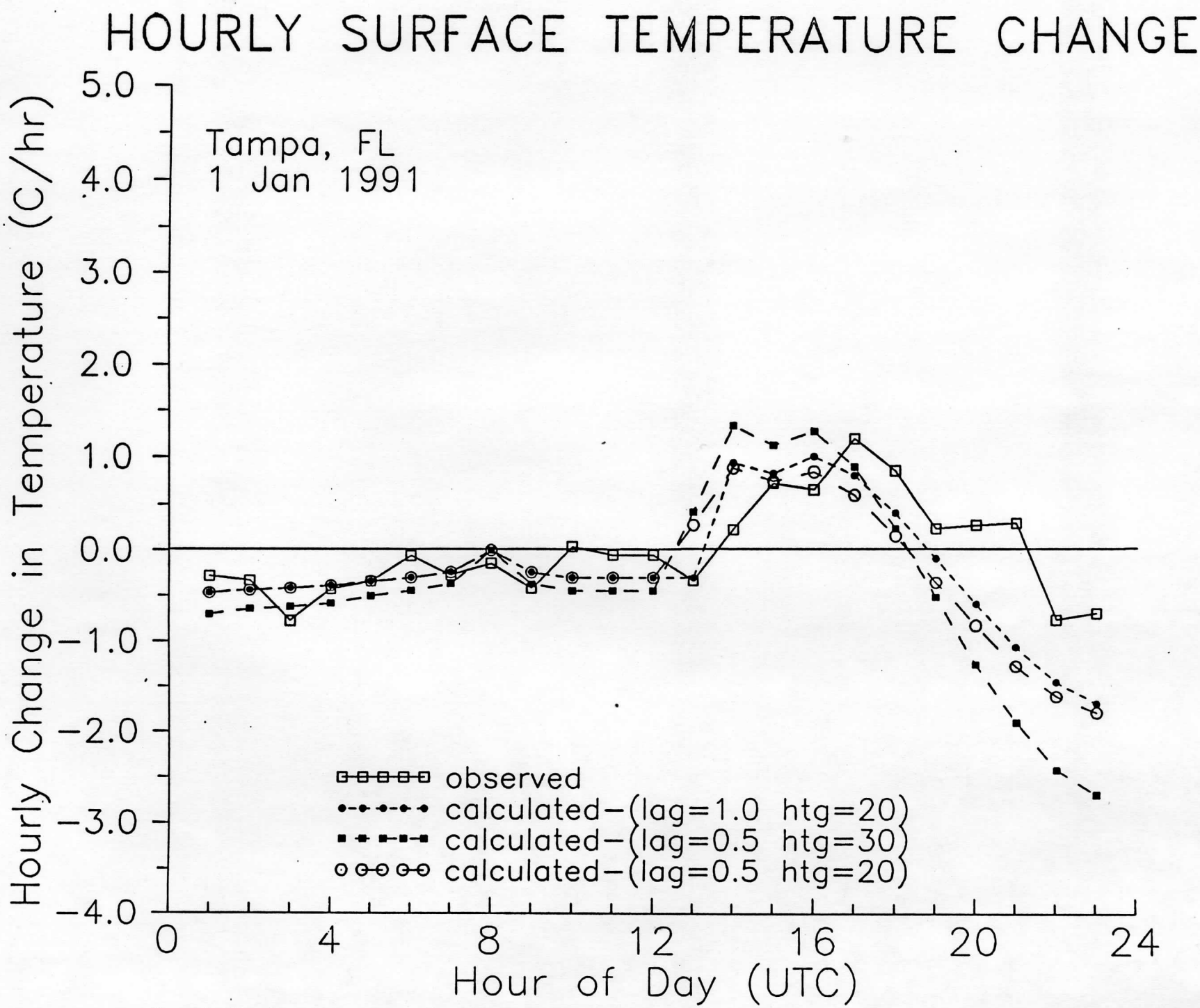

Figure 1. Hourly surface temperature change for Tampa, Fl. 1 Jan 1991. Hourly change in temperature for the current hour is derived by subtracting the previous hour from the current hour.

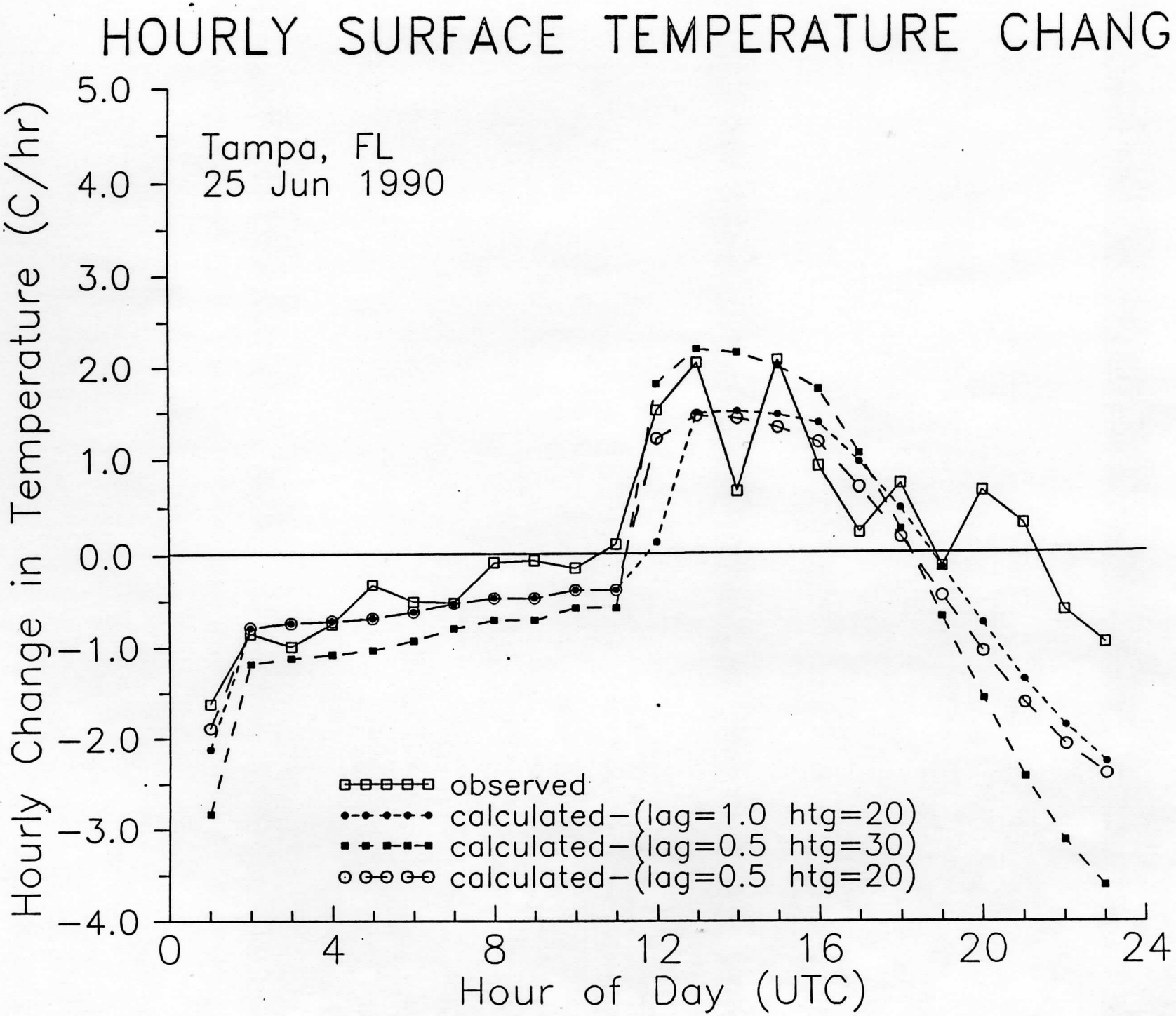

Figure 2. Same as Fig. 1 except for 25 Jun 1990.

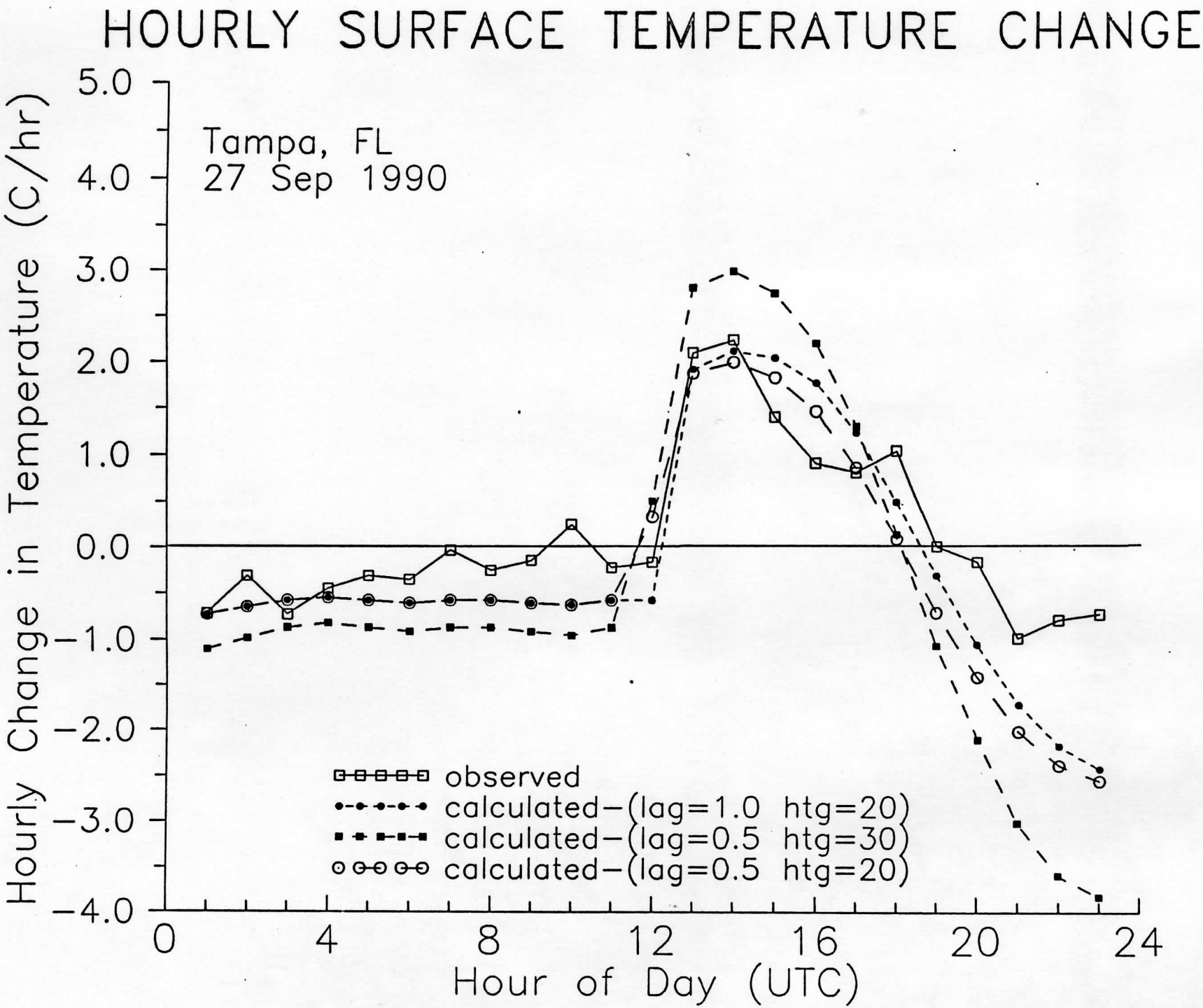

Figure 3. Same as Fig. 1 except for 27 Sep 1990.

H. VAS RETRIEVALS OF TEMPERATURE AND MOISTURE OVER SWAMP. Contribution by Christopher M. Hayden.

1. Introduction

In August of 1990, the SW Area Monsoon Project (SWAMP) conducted a field experiment in the Southwestern U. S. and Northwestern Mexico. There are three scientific objectives to this study: the Monsoon structure and moisture fluxes into the Southwest; the evolution of convective systems over Northern Mexico; and the generation of Central Arizona thunderstorms. All contribute significantly to the meteorology of the SW, and particularly to the important hydrological cycle.

The geographical area of concern to SWAMP is not well represented by routine observations. Therefore, a focus of the experiment was the deployment of the NOAA's P-3 aircraft over the regions of interest. Special CLASS rawinsonde launches were also used, but only in the Central Arizona phase. Even with these supplements, however, the observational network is inadequate to define the complex structure of the Monsoon or the convective systems, and it is quite natural to consider the applicability of remote sensing to the problem.

The Cooperative Institute for Meteorological Satellite Studies at the University of Wisconsin was peripherally involved with SWAMP and tasked with providing remote sensing support. This consisted of collecting DMSP SSM/I, AVHRR, and GOES-VAS data with the intention of processing these data as demand arose. We have subsequently had the opportunity of investigating the VAS data, and have been surprised by the variety of difficulties encountered in obtaining temperature and moisture profiles.

The area and season of SWAMP data contributed a number of features which complicate remote sounding. There are the usual cloud problems. Cirrus is prevalent, largely from orographically induced thunderstorm activity, and there is persistent marine stratus off the coast of California. Both of these cloud conditions are difficult to detect from infrared measurements. In addition, rugged topography, extreme surface temperature gradients, and surface temperatures in excess of 50 C are routinely encountered. Each of these challenges the temperature/moisture retrieval problem. The SWAMP data sets examined here have led to modifications of the operational VAS retrieval algorithm as described in Hayden (1988, hereafter referred to as I.). These changes are presented here.

2. Modifications to the Operational Retrieval Algorithm for SWAMP.

Modifications to the VAS retrieval algorithm for the processing of the SWAMP data involved three aspects of the retrieval program:

Cloud clearing and sampling

The standard practice with the VAS has been to process the measurements as 11 x 11 fields-of-view (fov), offering the opportunity for cloud clearing by "hole seeking", and horizontal averaging to

improve signal-to-noise. The sample to be averaged is restricted to a variance commensurate with instrument noise combined with anticipated natural atmospheric variance over the (approximately) 100 x 100 km scene. Furthermore, to maximize the sample, each of the 12 bands is treated independently, i.e. with no restriction of co-registration. Finally because the VAS yields a somewhat noisy measurement, 25 cloud cleared fov are required for averaging before a temperature retrieval is attempted.

In processing the SWAMP data we discovered that although the algorithm produced cloud cleared radiances, the retrievals were rarely successful, in a large measure because one or more bands failed the convergence test which requires that calculated and observed brightness temperatures agree within specified limits. (These limits vary from channel to channel according to their noise characteristics.) A majority of the failures involved channels with a large contribution from the surface, suggesting that extreme variation in topography and skin temperature was the problem. The cloud clearing algorithm was therefore modified to include co-registration of the two long wave window channels (11.2 and 12.4 micrometers) with optional co-registration for the other channels, excepting the two most opaque (and noisy), bands 1 and 2. Each channel is still independently filtered as before, but a failure in any co-registered channel now eliminates the measurement for all co-registered channels. Naturally, the number of 11 x 11 "boxes" failing to achieve the minimum sample size is increased by the co-registration requirement, especially as additional channels are included, but the number of successful retrievals was significantly increased, and the changes to the first guess profiles somewhat reduced (which is usually a good sign.)

Emissivity correction

Until the time of the SWAMP experiment, The VAS retrieval algorithm used a fixed surface emissivity of 1.00 over water and cloud and of .99 over land. (Originally, a constant emissivity of 0.96 was used over land for the justification given in (I). In 1988 the value was changed to a more physically realistic 0.99 without noticeable degradation in the retrievals.) In general, the retrieval is not highly sensitive to small variations in surface emissivity, particularly when modifying an accurate first guess profile, but sensitivity increases as humidity decreases and the surface signal increases. Because of the hot surface temperatures encountered with the SWAMP data, the algorithm was altered to permit a variable surface emissivity, and also to include the reflected atmospheric component previously ignored in (I).

The procedure for including a variable emissivity is as follows. Following cloud clearing, the surface skin temperature is estimated by a two or three channel "split window" regression as described in (I). A transmittance profile for the 11 micrometer window is estimated from the first guess temperature and moisture profiles. These are used to calculate the outgoing radiation for the window channel which can be compared to the observation. The comparison gives a first estimate of the emissivity as shown in (1)

$$\varepsilon_\nu = \frac{R_\nu - \int_{\tau_s}^{1} B_\nu(T_p)\,d\tau_{\nu p} - \int_{\tau_s}^{1} \left(\frac{\tau_{sp}}{\tau_{\nu p}}\right)^2 B_\nu(T_p)\,d\tau_{\nu p}}{B_\nu(T_s)\,\tau_{\nu s} - \int_{\tau_s}^{1} \left(\frac{\tau_{sp}}{\tau_{\nu p}}\right)^2 B_\nu(T_p)\,d\tau_{\nu p}} \qquad (1)$$

The variables of (1) are described in the Appendix. There are two major uncertainties involved in the calculation of the r.h.s of (1) ; the low level moisture profile which effects the transmittance and the surface temperature. Thus the initial estimate may be quite inaccurate, and it is not unusual to obtain estimates of emissivity as low as .9 or as high as 1.2. Obviously these are physically unrealistic, and they are trapped at unity on the high end and at 0.98 on the low end. The trapped emissivity is then used to re-estimate the surface skin temperature before beginning the retrieval as described in (I) with the modifications given in the Appendix. Both the new emissivity and skin temperature affect the initial calculation of radiance temperatures for channels which sense the surface. When iterating the retrieval, and for the SWAMP data we used three iterations, the emissivity is recalculated after each iteration using the retrieved skin temperature. However, the calculated value is still trapped, and that may lead again to a modification of the skin temperature.

Reflected solar radiation.

Reflected solar radiation is another term in the radiative transfer equation which has been ignored in VAS processing. The justification is that the 3.95 micrometer short wave window is not used during the day, and the other short wave channels at 4.52 and 4.48 micrometers do not have a large surface component. Because of the strong solar component in the SWAMP data we also relaxed this assumption. However, we found that the correction remained completely negligible.

In addition to the changes above made explicitly for these data sets, the SWAMP experiment also was one of the first processed with an updated bias correction scheme which has subsequently been included in the operational processing.

Bias Correction.

The existence of bias errors in the forward calculation of radiances, caused by uncertainties in transmittances and by the lack of vertical resolution, is a well known problem in physical retrievals. As described in (I), the VAS retrieval prior to 1992 addressed the problem by applying a bias vector to the measurements. The vector was derived from a sample of differences between observation and the brightness temperature calculated from the NMC forecast as modified to provide the first guess profiles. This computation was made immediately prior to making retrievals using a sample drawn from the full domain of the current set of observations.

The new bias correction procedure follows a method suggested by Fleming (1991). The method involves constrained regression whereby many channels are used to predict the correction of a given channel. The constraint requires that the channel itself be the principal predictor, since otherwise inter-atmospheric correlations lead to a logically unrealistic result. The correction is also constrained to the variance contained in a sample of calculated radiance temperatures. The advantage anticipated from the newer method is that the bias correction becomes air mass dependent, since it can vary over the domain. The main drawback to the newer method is that it is not clearly an advantage to adjust the observed variance to the calculated, particularly for channels where the calculation is suspect. This point is briefly addressed in the results below. In the new method, the tropospheric water vapor channels, the 6.7 and 7.2 micrometer bands, are now being corrected whereas previously they were not. This change means that they can now also be used in the retrieval quality control which requires that (bias corrected) observation agree with the brightness radiance calculated from the retrieval within "noise". We experimented with correcting the window channels as well (the 11.2 and 12.7 micrometer bands), but their corrections behaved erratically, and they continue to be used uncorrected as before. Dependent samples are still comprised of observations vs. radiance temperatures calculated from first guess profiles. Unlike the earlier method, the dependent samples are collected over many days, and the coefficients are updated infrequently.

3. Results

The situation over the SWAMP experiment region on 5 August, 1990 is shown in Fig. 1. The 11.2 micrometer window and 6.7 micrometer water vapor band are both presented as observed at 01:01 UT. Typical convective cloudiness, generally orographically induced in the late afternoon, is seen, as well as the extreme surface temperatures in the western U.S. Marine stratus is seen off the coast. The water vapor channel indicates little about the moisture pattern, except to suggest slight subsidence drying west of the Baja peninsula and general upper level moisture associated with the convection. Fig. 2 shows the magnitudes of the radiance temperatures for the 6.7 micrometer channel, both the first guess (upper left) and for the observation (upper right) These analyses are prepared from cloud cleared observations and are therefore credible only where the data are indicated. The warmer temperatures observed in Fig. 1 are also seen in the analysis of the observations.

Fig. 2 also shows the characteristics of the bias correction currently applied in the VAS algorithm as explained above. The bias (to be added to the observation) is shown by the dashed line in the upper right for the 01:48 UT case. Note that it varies from approximately 1K in the colder region to more than 4K in the warm subsidence region. Note also that the correction has increased the horizontal variance, probably incorrectly since this band fails the quality control (bold 10's plotted in the figure) where the bias correction is largest, and the failure is caused because the bias-corrected radiance temperature is too warm relative to that calculated from the retrieval (lower left figure). Indeed, the contour pattern of the retrieval looks closer to the pattern of the uncorrected channel. Based on this and other experiments, the question of the

appropriateness of correcting the water vapor channels is still moot.

The retrieved skin temperatures for the three periods processed are shown in Fig. 3. In each of these the surface emissivity was limited to be no less than 0.98. Two factors are of special interest. First, note the extreme temperature changes over southern California and the Baja as the sun sets. Changes of greater than 20C in the three hours are not uncommon. Second, note the poor coverage obtained at 22:48 UT on 4 August, relative to the later periods. The relative paucity is directly related to the heterogeneous surface conditions. When the minimum required fov sample was reduced from 25 to 16, the yield at 22:48 UT rose to approximate that of the later periods. There remained a larger percentage of retrieval failures, mostly over the hot surface, and these were generally attributed to the most transparent channels. The accuracy of the successful retrievals did not appear, qualitatively, to be degraded by the reduced sample, but that is not surprising since the noise reduction factor changes only from 5 to 4. The more remarkable feature is that one can get a homogenous sample of only 16 out of a possible 121.

Fig. 4 shows the result of testing the limit on surface emissivity. The test was performed on the 01:48 UT case. The two upper figures represent limits of 0.96 (left) and 0.99 (right). Only retrievals passing quality control checks are shown. It is apparent that the change in emissivity limit affected the coverage very little. It is also seen that the retrieval usually accepted all leeway when the emissivity was limited to 0.96. The effect on the retrieved temperature is relatively small, as shown in the lower left figure. In the hot ground cases the lower emissivity cools the retrieval 850 hPa temperature a few tenths of a degree. As might be anticipated, given the poor vertical resolution of the retrieval, this change is quite uniformly distributed throughout the lower troposphere (below 500 hPa). Our conclusion from this exercise is that the change caused by allowing the emissivity to fall to 0.96 is too small to justify what seems to be an unrealistically low limit, even though the algorithm accepts it.

Statistics relating the retrievals (and the first guess) for the 01:48 UT period with the rawinsonde measurements of 00 UT are presented in Table 1. As we have found in the past, the accuracy of the retrievals is approximately the same as that of the first guess. The sample is small, the atmospheric variance is low, it is difficult to draw conclusions. It does appear that the VAS retrieval may be a bit too warm and too dry in the lower troposphere, suggesting that the hot skin is having too much influence.

Table 1: Statistical comparisons, Rawinsonde/VAS retrieval matched profiles for 01:48 UT retrieval set. (14 matches within 75 km).

	VAS			First Guess		
	Temperature					
level	Mean	RMS	CC	Mean	RMS	CC
850	1.6	2.0	.95	0.9	2.1	.83
700	0.2	1.0	.81	-0,8	1.0	.57
500	0.8	1.1	.69	0.0	0.8	.65
400	-0.9	1.4	.72	-1.5	1.7	.86
300	-0.1	1.4	.81	-0.4	1.2	.94
	Dew point					
level	Mean	RMS	CC	Mean	RMS	CC
850	-1.7	5.7	.89	-0.2	2.8	.89
700	-1.6	4.4	.90	-0.6	4.6	.85
500	-1.2	6.1	.83	-2.1	5.2	.89
400	2,0	7.7	.62	1.9	5.9	.80
300	-5.0	7.1	.67	-9.0	16.	.28

It is usually more meaningful to compare objective analyses of the retrievals with the first guess, and this is done in Figs. 5 through 7. Figure 5 shows the 850 hPa temperature fields and the difference. It is apparent that the retrievals have had a significant effect only over the warm surface, and the 850 hPa temperatures have been raised as much as 3K. As seen in Table 1 the rawinsondes suggest that the warming is a bit pronounced, but probably not much. As shown previously, lowering the surface emissivity only modifies the warming by a few tenths of a degree.

Figs. 6 and 7 show the retrieved change in precipitable water for the lowest 100 hPa and the total column, respectively. At low levels, as compared to the first guess, the VAS indicates drying west of Baja with quite strong moistening along the western Mexican coast. The pattern is quite different from the heating pattern shown in Fig. 5, thus the retrievals are offering independent information on temperature and moisture, as they should. Looking at the change in the total column moisture in Fig. 7, it is apparent that the retrievals have had a strong impact on the gradient in the Gulf of California. One also sees the previously reported (Rabin et al., 1992) vertical differentiation in the moisture by comparing the change in low level precipitable water (Fig. 6) with the change in the total column. The reader might note that the total column value for the rawinsonde at Guaymas is not shown in Fig. 7. Unfortunately it did not report enough levels of information to satisfy our criteria.

4. Summary

The SWAMP data sets offered an interesting challenge to the VAS operational algorithm for retrieving profiles of temperature and moisture. A number of changes were instituted to accommodate these data, and although these changes did not have a large impact on the retrievals, we believe they are an improvement. At the very least we gained a better appreciation of the impact of surface emissivity, co-registration, and high skin temperatures. Although it is very difficult to verify that changes indicated by the retrievals are accurate, we are quite satisfied with the results as they seem qualitatively reasonable. Spatial and temporal continuity are excellent, and the largest changes are made where they would seem most probable.

Appendix

The radiative transfer equation is given by:

$$R_\nu = B_\nu(T_s)\,\tau_{\nu s}\varepsilon_\nu + \int_{\tau_s}^{1} B_\nu(T_p)\,d\tau_{\nu p} + (1-\varepsilon)\int_{\tau_s}^{1}\left(\frac{\tau_{sp}}{\tau_{\nu p}}\right)^2 B_\nu(T_p)\,d\tau_{\nu p} \tag{1A}$$

where R is radiance, B is radiance temperature, t is transmittance , T is temperature , p is pressure, ν is spectral frequency, and ε is the surface emissivity. Subscript s refers to the earth's surface. The three terms on the r.h.s. of (1A) are, respectively, the surface term, the upwelling atmospheric term, and the reflected atmospheric term. The last two terms can be combined to give:

$$R_\nu = B_\nu(T_s)\,\tau_{\nu s}\varepsilon_\nu + \int_{\tau_s}^{1}\left[1+(1-\varepsilon)\left(\frac{\tau_{sp}}{\tau_{\nu p}}\right)^2\right] B_\nu(T_p)\,d\tau_{\nu p}\,. \tag{2A}$$

The first step in solving (1A) is to linearize around a basic state, usually called the first guess:

$$R - R^0 = B_s\tau_s - B_s^0\tau_s^0 - \int_{\tau_s}^{1} \mathrm{R}_f B\,d\tau + \int_{\tau_s}^{1} \mathrm{R}_f^0 B^0\,d\tau^0 \tag{3A}$$

where superscript 0 refers to the basic state and:

$$\mathrm{R}_f = \left[1+(1-\varepsilon)\left(\frac{\tau_{sp}}{\tau_{\nu p}}\right)^2\right]. \tag{4A}$$

Frequency and pressure designations have been eliminated for simplicity. Letting

$\tau = \tau^0 + \delta\tau$, $\delta R = R - R^0$; $\delta B = B - B^o$

$$\delta R = \delta B_s\tau_s^0 + B_s\delta\tau_s - \int_{\tau_s}^{1}(\mathrm{R}_f B - \mathrm{R}_f^0 B^0)\,d\tau^0 - \int_{\tau_s}^{1}\mathrm{R}_f B\,d(\delta\tau) \tag{5A}$$

Integrating the last term by parts:

$$-\int_{\tau_s}^{1}\mathrm{R}_f B\,d(\delta\tau) = \mathrm{R}_f B\delta\tau\Big|_{\tau_s}^{1} + \int_{\tau_s}^{1}\mathrm{R}_f\delta\tau\,dB \tag{6A}$$

(5A) becomes:

$$\delta R = \varepsilon \delta B_s \tau_s^0 - \int_{\tau_s}^{1} (\mathrm{R}_f B - \mathrm{R}_f^0 B^0) d\tau^0 + (B_s - B_a)\mathrm{R}_f \delta\tau_s + \int_{\tau_s}^{1} \mathrm{R}_f \delta\tau dB \qquad (7A)$$

where subscript a refers to surface air as distinct from surface skin temperature. The terms involving R_f and B_a introduce intractable non-linearities in (7A) so we make the initial assumptions that:

$$R_f = R_f^0 \qquad \delta\tau_s = \delta\tau_s^0 \qquad B_a = B_a^o \qquad (8A)$$

These assumptions can be mitigated by iterating the solution of (6A) whereby the superscript zero then applies to the result of the previous iteration. Then

$$\delta R = \varepsilon \delta B_s \tau_s^0 - \int_{\tau_s}^{1} \mathrm{R}_f^0 \delta B d\tau^0 + (B_s - B_a^0)\mathrm{R}_{fs}^0 \delta\tau_s^0 + \int_{\tau_s}^{1} \mathrm{R}_f^0 \delta\tau dB. \qquad (9A)$$

The third term on the r.h.s. can be folded into the second as the quadrature is performed and this can be expressed by changing the lower limit of the integral:

$$\delta R = \varepsilon \delta B_s \tau_s^0 - \int_{\tau_s}^{1} \mathrm{R}_f^0 \delta B d\tau^0 + \int_{\tau_s}^{1} \mathrm{R}_f^0 \delta\tau dB^0 . \qquad (10A)$$

Note also the superscript added in the last term such that the integration involves only first guess quantities. Further linearization makes use of:

$$\begin{aligned} \delta R &= \delta T_b \partial B^0 / \partial T_b^0 \\ \delta B &= \delta T \partial B^0 / \partial T^0 \\ \delta\tau^0 &= \frac{\partial \tau^0}{\partial \ln u^0} d\ln u = \frac{1}{u}\left(\frac{\partial \tau}{\partial \ln u}\right) du \end{aligned} \qquad (11A)$$

such that (10A) may be expressed:

$$\delta T_B = \delta T_s \frac{\partial B_s}{\partial T_s} \varepsilon \tau_s^0 - \int_0^{P_s'} \delta T \mathrm{R}_f^0 \left(\frac{(\partial B^0 / \partial T^0)}{(\partial B^0 / \partial T_b)}\right) \mathrm{d}\tau^0 + \int_0^{P_s} \delta u \left(\frac{1}{u^0} \frac{\partial \tau^0}{\partial \ln u^0}\right) \mathrm{R}_f \left(\frac{(\partial B^0 / \partial T^0)}{(\partial B^0 / \partial T_b)}\right) \mathrm{d}T^0 \qquad (12A)$$

which is in the same form as (1) in (I).

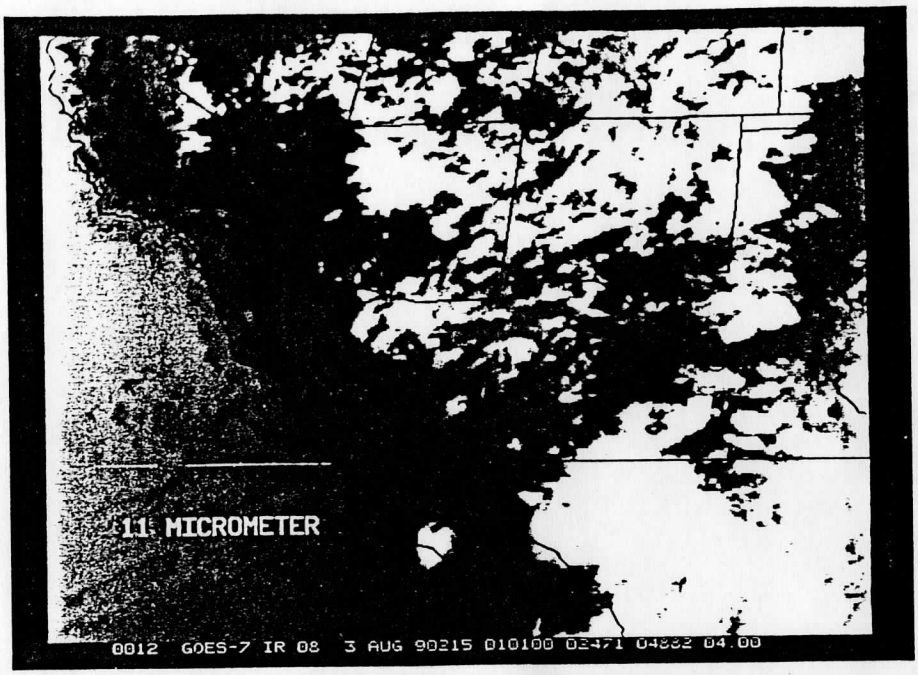

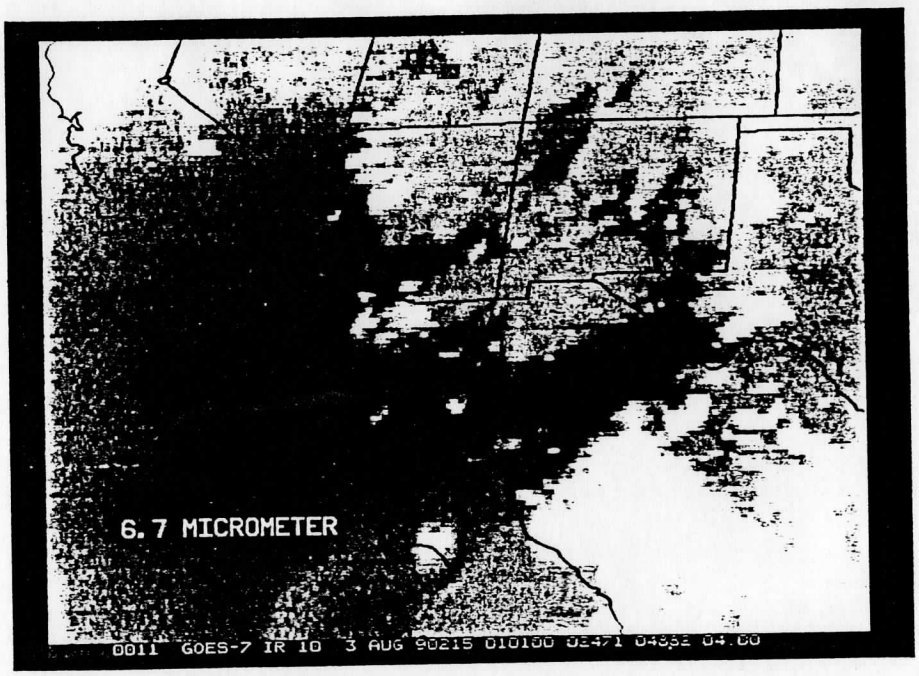

Fig. 1. 11 and 6.7 micrometer radiances for SWAMP case of 5 August, 1992, 01:01 UT.

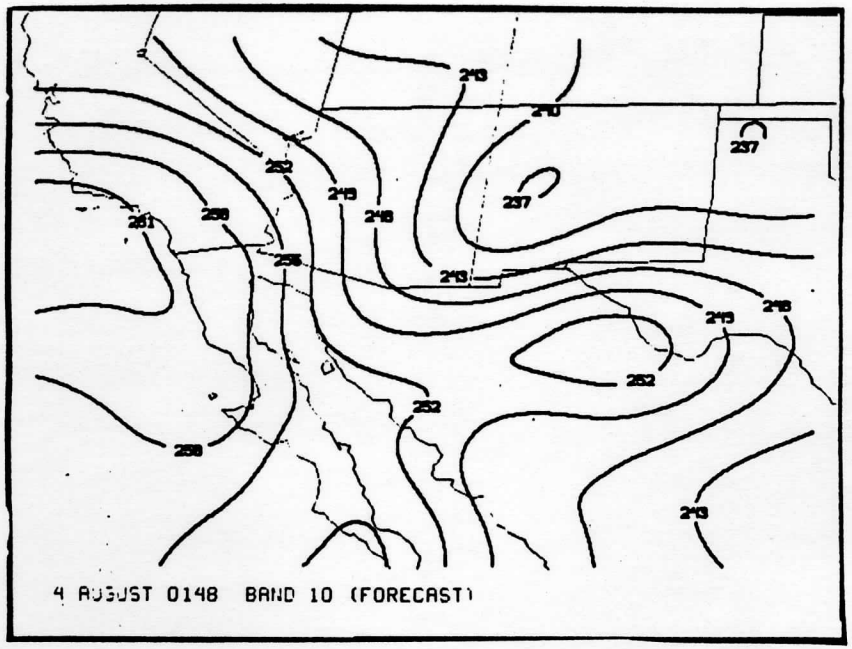

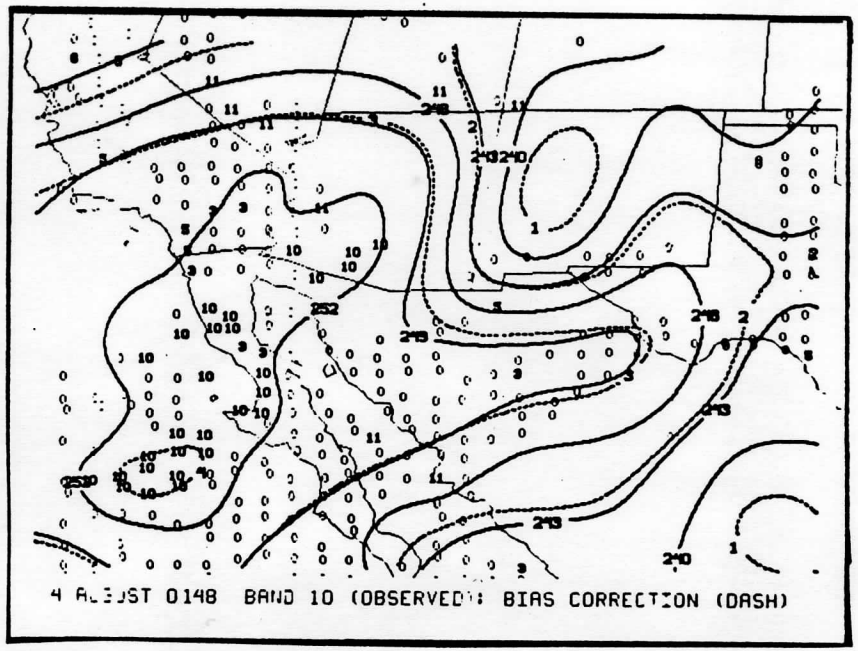

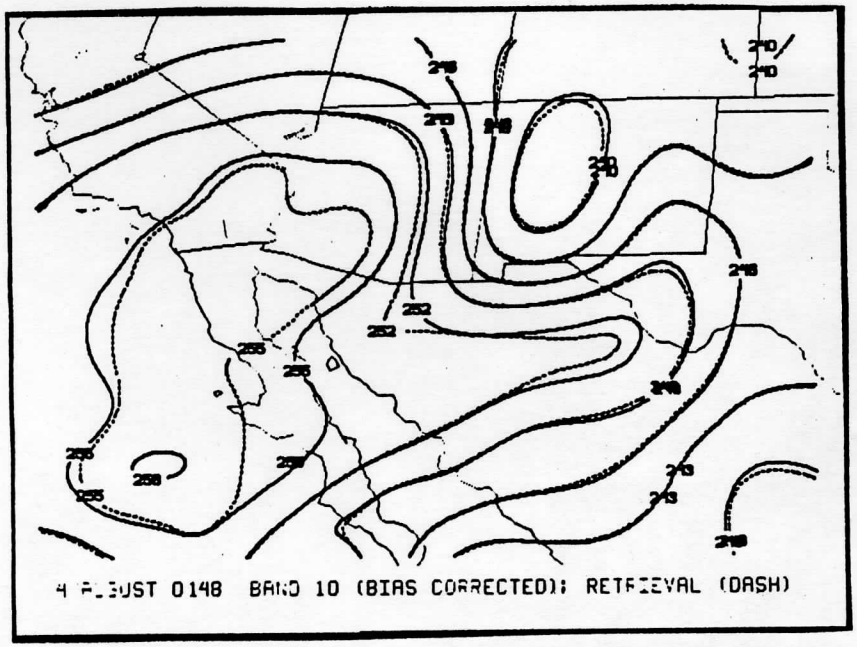

Fig. 2. 6.7 micrometer bias correction. Upper left: radiance temperature calculated from first guess. Upper right: observed radiance temperature and bias correction (dashed). Locations of attempted retrievals are shown; bold indicates a channel causing retrieval failure. Lower left: bias corrected observation and radiance temperature calculated from retrievals.

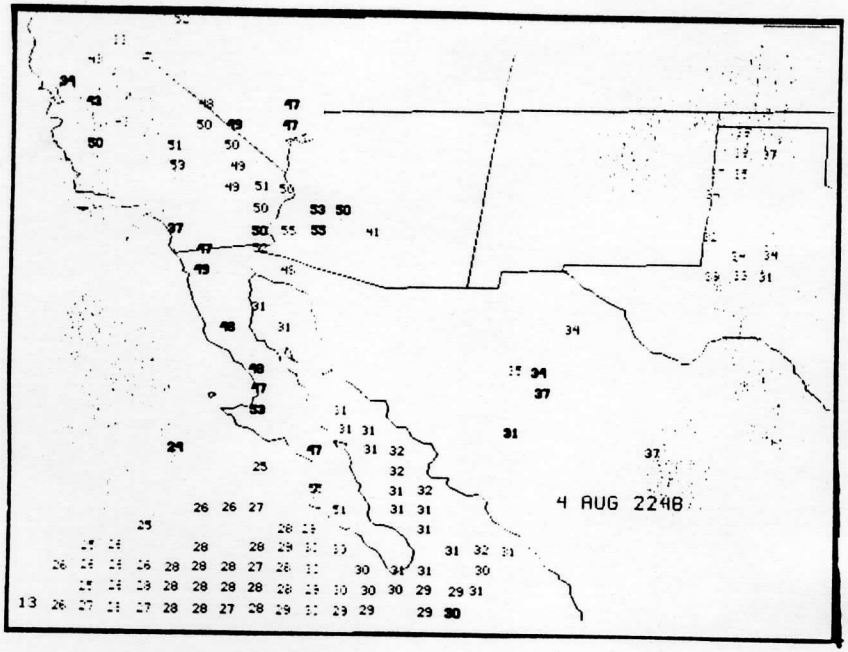

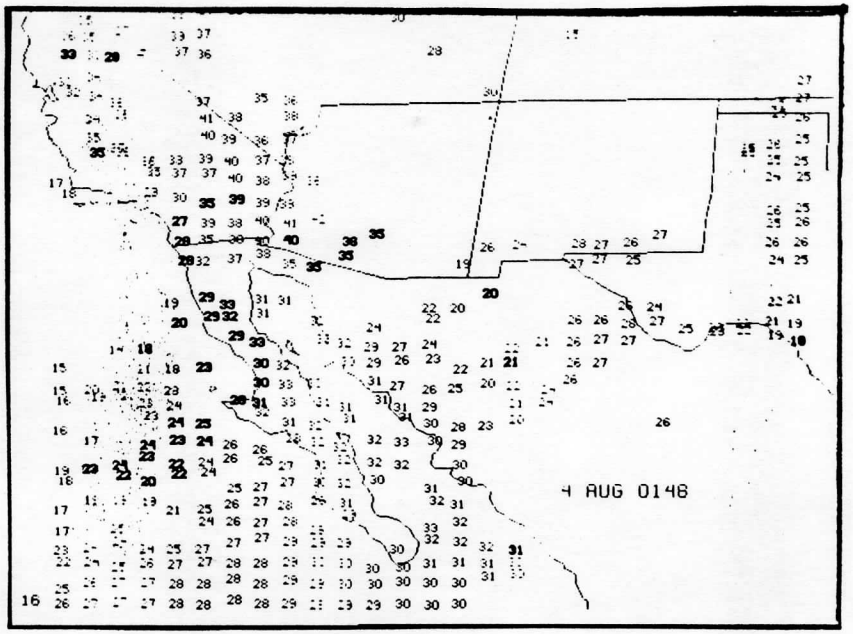

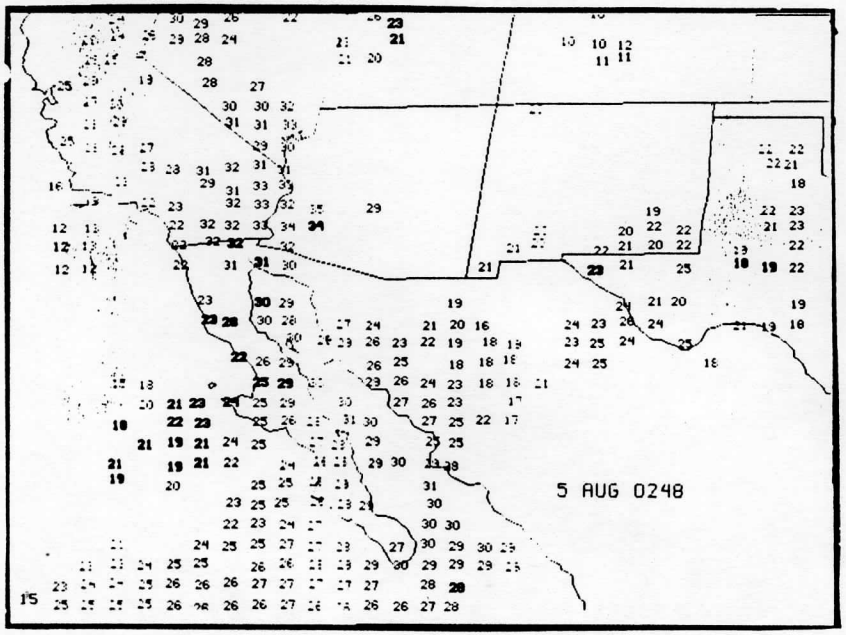

Fig. 3. Surface skin temperatures calculated for 3 time periods. Bold indicates quality control failure.

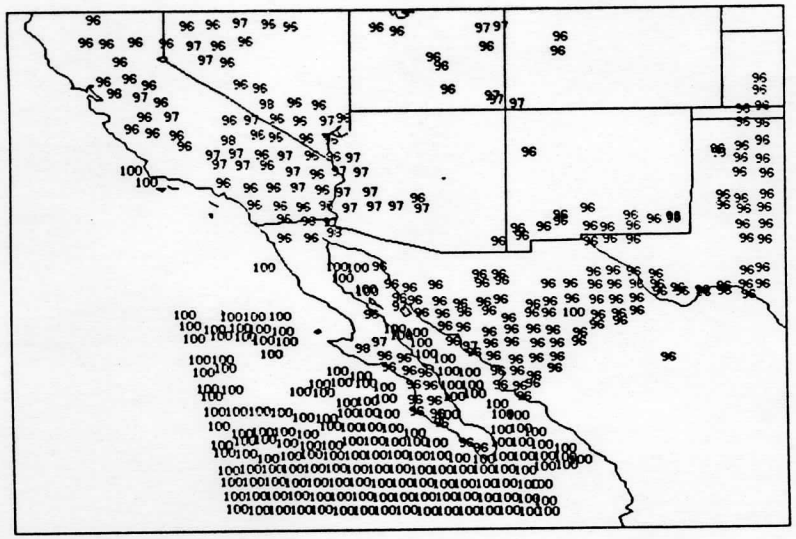

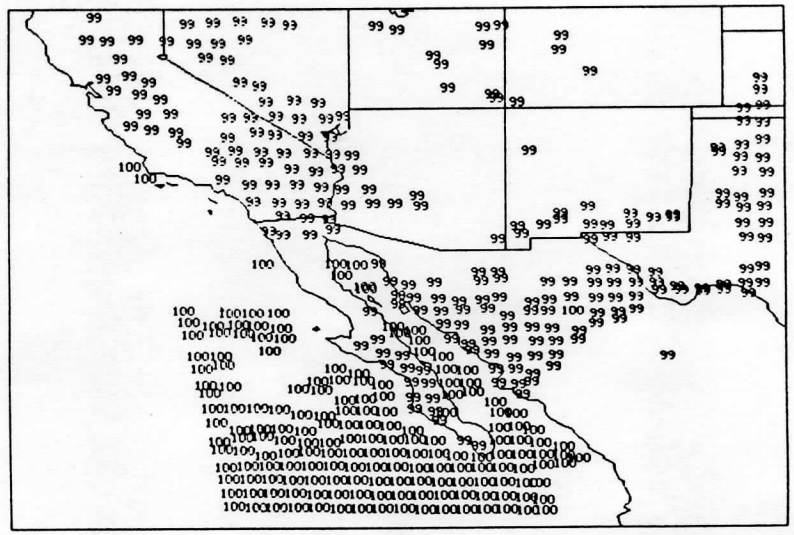

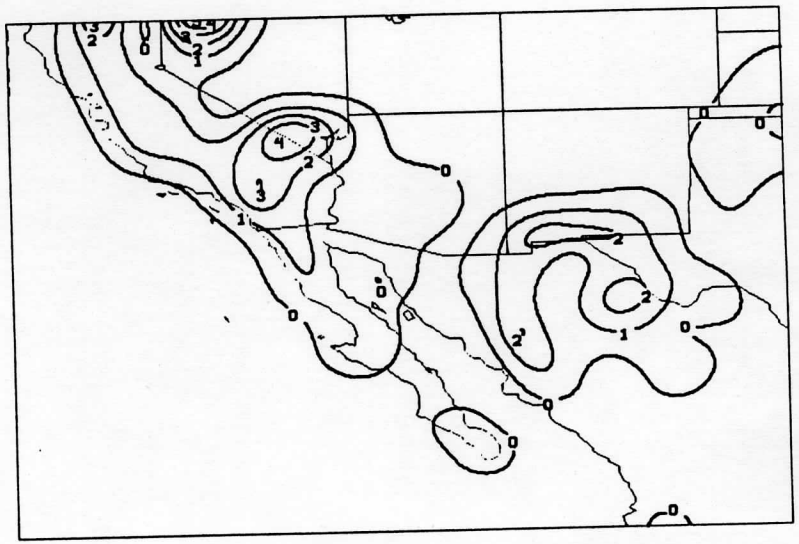

Fig. 4. Retrieved emissivities when upper limit is capped at .96 (upper left) and .99 (upper right). Difference in retrieved 850 hPa temperatures (.99 - .96) is shown in lower left. Units are K*10.

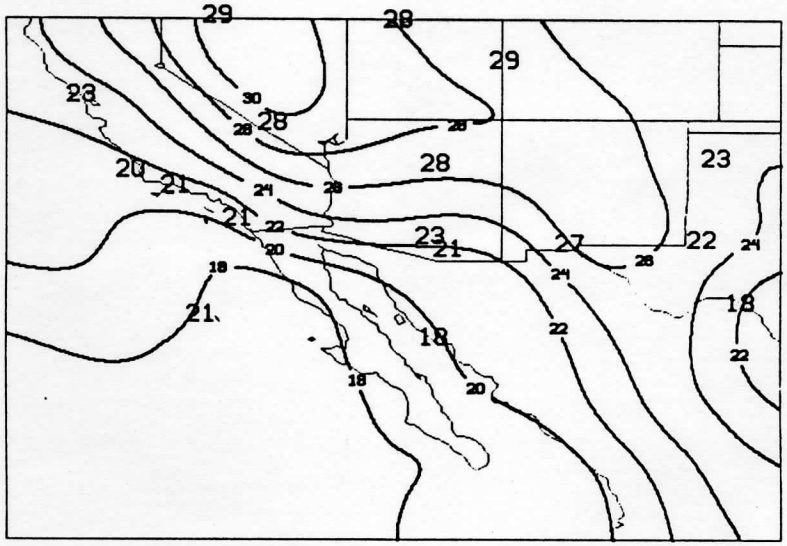

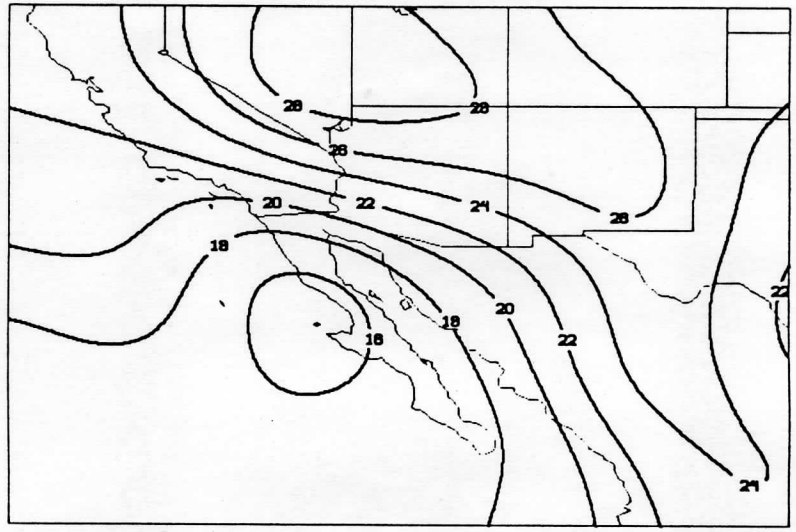

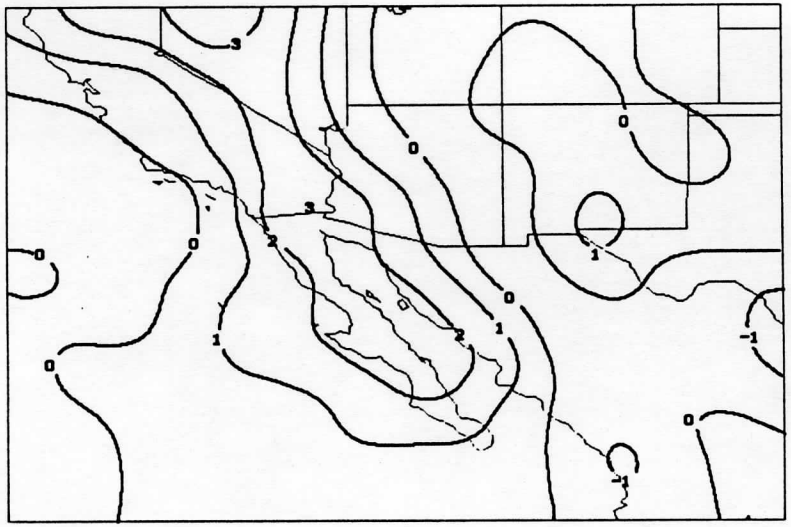

Fig. 5. Upper left: Retrieved 850 hPa field for 01:48 UT. 00 UT radiosonde observations are also shown. Upper right: First guess (NMC forecast) 850 hPa field. Lower left: retrieval minus first guess. Units are C.

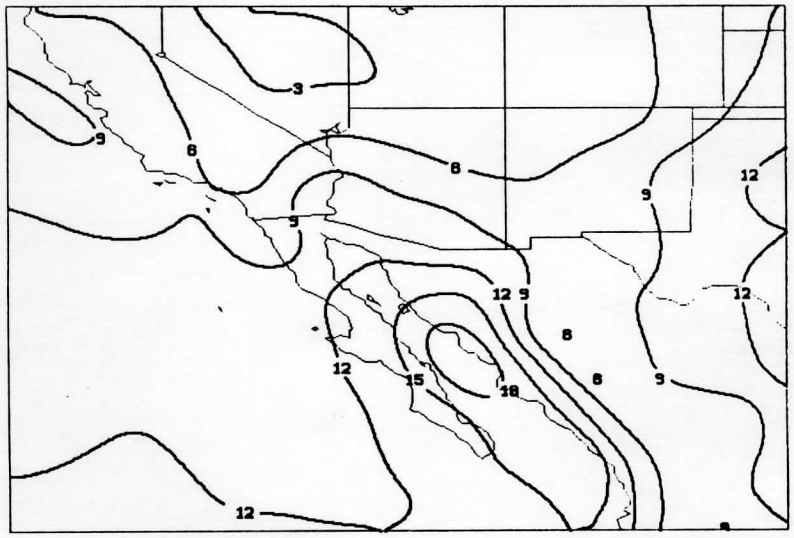

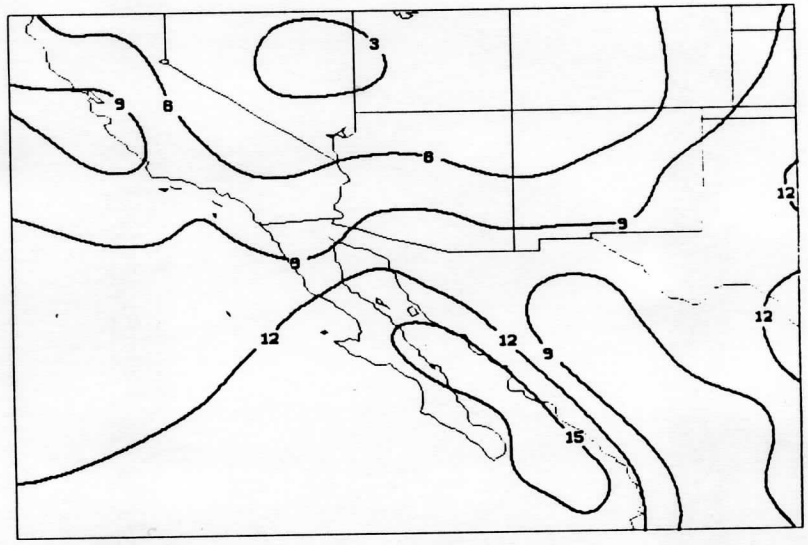

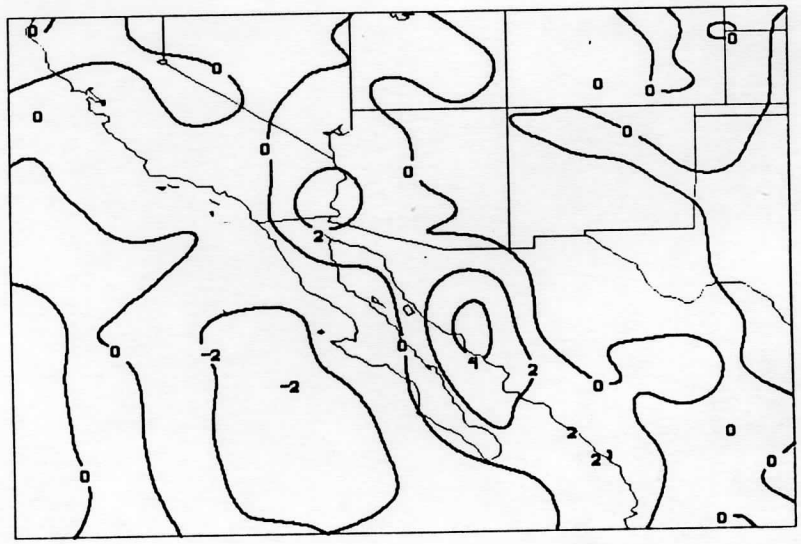

Fig. 6. Upper left: Retrieved low level (sigma=.9, sigma=P/P_S) . Upper right: First guess low level precipitalbe water. Lower left: retrieval minus first guess. Units are mm.

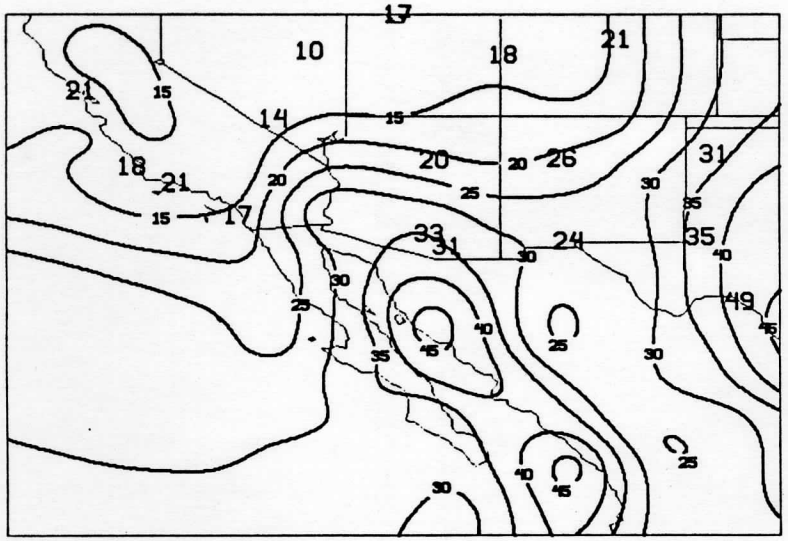

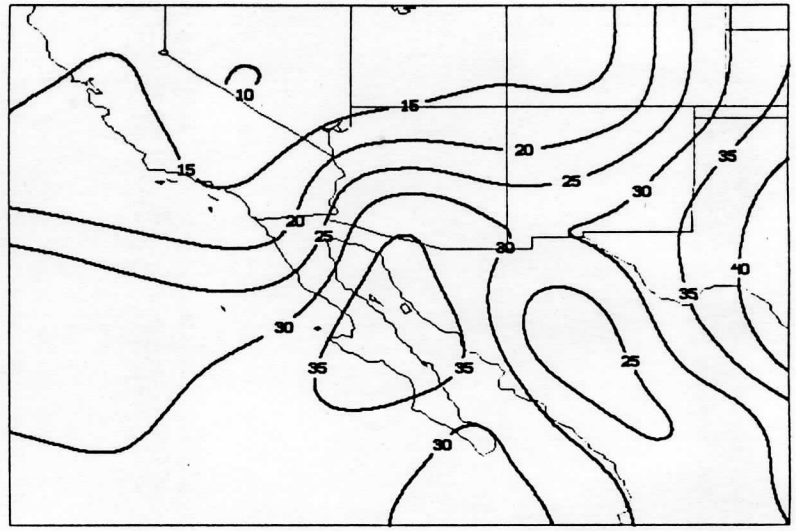

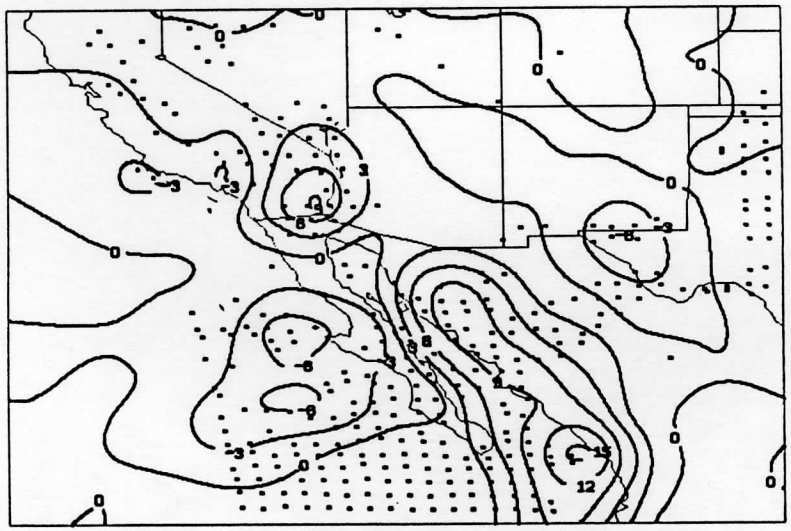

Fig. 7. Upper left: Retrieved total precipitable water for 01:48 UT. 00 UT radiosonde observations are plotted. Upper right: First guess total precipitable water. Lower left: retrieval minus first guess.

I. METEOROLOGICAL DATA ASSIMILATION BY ADAPTIVE BAYESIAN OPTIMIZATION. Contribution by R. James Purser.

(Ed. note: The following is the abstract of Dr. Purser's Ph.D. thesis. Dr. Purser was supported by the Severe Weather Program throughout his studies at the University of Wisconsin. He is currently visiting the National Meteorological Center on a UCAR post-doctoral fellowship.)

The principal aim of this research is the elucidation of the Bayesian statistical principles that underlie the theory of objective meteorological analysis. In particular, emphasis is given to aspects of data assimilation that can benefit from an iterative numerical strategy. Two such aspects that are given special consideration are statistical validation of the covariance profiles and nonlinear initialization.

A new economic algorithm is presented, based on the imposition of a sparse matrix structure for all covariances and precisions held during the computations. It is shown that very large data sets may be accommodated using this structure and a good linear approximation to the analysis equations established without the need to unnaturally fragment the problem. Since the integrity of the system of analysis equations is preserved, it is a relatively straight-forward matter to extend the basic analysis algorithm to one that incorporates a check on the plausibility of the statistical model assumed for background errors - the so-called "validation" problem. Two methods of validation are described within the sparse matrix framework: the first is essentially a direct extension of the Bayesian principles to embrace, not only the regular analysis variables, but also the parameters that determine the precise form of the covariance functions; the second technique is the non-Bayesians method of generalized cross validation adapted for use within the sparse matrix framework.

The later part of this study is concerned with establishment of a consistent dynamical balance within a forecast - the initialization problem. The formal principles of the modern theory of initialization are reviewed and a critical examination is made of the concept of the "slow manifold." It is demonstrated, in accordance with more complete nonlinear models, that even within a simple three-mode linearized system, the notion that a universal slow manifold exists is untenable. It is therefore argued that a consistent treatment of the initialization problem should strictly be guided by statistics as much as by dynamics; a new methodology to accomplish the unification of analysis and initialization within the Bayesian paradigm is proposed (Purser, 1992).

III. PERSONNEL AND EQUIPMENT

Personnel

	LABOR (%)	COMPUTER (%)
SSEC		
Anthony J. Schreiner	20	30
R. James Purser	50	0
Barry Rowe	20	20
Timothy J. Schmit	10	15
Christopher S. Velden	10	10
Xiaohua Wu	100	100
NESDIS		
Christopher M. Hayden		20
Gary S. Wade		40
Robert M. Aune		85
Leroy D. Herman		90
Geary M. Callan		40
Robert M. Rabin		20

The numbers underneath the column "LABOR" represent the percentage of their labor time which was charged to this project. The percentages below the column headed by "COMPUTER" indicate the amount of computer time which the scientists charged to this contract. Both percentages are based on one year being equivalent to 100%. NESDIS employees' labor is provided from funds outside of this contract.

Equipment

None

IV. SUMMARY

The support from this contract has been important in providing the programmers, research scientists, and support staff the opportunity to perform a wide variety of research within the CIMSS organization. Many of the areas of research which were discussed in Section III are ongoing topics.

V. REFERENCES

Bourke, W. and J. McGregor, 1983: A nonlinear vertical mode initialization scheme for a limited area prediction model. *Mon. Wea. Rev.*, 111, pp 2285-2287

Diak, G.R., D. Kim, M.S. Whipple and X.H. Wu, 1992: Preparing for the AMSU. *Bull. Amer. Meteor. Soc.*, 73, 1971-1984.

Fleming, H. E., N. C. Grody, and E. J. Kratz, 1991: The forward problem and corrections for the SSM/T satellite microwave temperature sounder. IEEE Transactions on Geoscience and Remote Sensing 29, 571-583.

Hayden, C. M., 1988: GOES-VAS simultaneous temperature-moisture retrieval algorithm. J. Appl. Meteor., 27, 705-733.

Herman, L.D., 1991: The current state of development of a method of producing cloud motion vectors at high latitudes from NOAA satellites. Workshop on Wind Extraction from Operational Meteorological Satellite Data, Washington, D.C., 17-19 Sept. 1991.

Hibbard, W. and D. Santek, 1990: The VIS-5D for easy interactive visualization. *Visualization '90*, San Francisco, IEEE, pp 28-35.

Kasahara, A., A.P. Mizziand, and L.J. Donner, 1992: Impact of cumulus initialization on the spin up of precipitation forecasts in the tropics. *Mon. Wea. Rev.*, 120, 1360-1380.

Leslie, L. M., G. A. Mills, L. W. Logan, D. J. Gauntlett, G. A. Kelly, M. J. Manton, J. L. McGregor and J. M. Sardie, 1985: A high-resolution primitive equations model for operations and research. *Aust. Meteor. Mag.*, 33, pp 11-35.

Rabin, R.M., L.A. McMurdie, C.M. Hayden, and G.S. Wade, 1992: Layered precipitable water from the infrared VAS sounder during a return-flow even over the Gulf of Mexico. *J. Appl. Meteor.*, 31, 819-830.

Rabin, R.M., L.A. McMurdie, C.M. Hayden, and G.S. Wade, 1993: Evaluation of the atmospheric water budget following an intense cold-air outbreak over observations. *J. Appl. Meteor.*, 32, 3-16.

Seaman, R. S., R. L. Falconer, and J. Brown, 1977: Application of a variational blending technique to numerical analysis in the Australian region. *Aust. Meteor. Mag.*, 25, pp 3-23.

Turner, J. and D.E. Warren, 1989: Cloud track winds in the polar regions from sequences of AVHRR images. Int. *J. Remote Sensing*, 10, 695-703.

Wade, G.S., 1992: Precipitable water fields derived from VAS data over the Southwest. Fourth Arizona Weather Symposium. Phoenix, AZ., 10-12 June 1992.

Wu, X.H., 1991: Short-time precipitation forecast using assimilation of satellite-observed water vapor, liquid water and surface rain rates. A proposal for Ph.D. dissertation, University of Wisconsin-Madison.